SRI International

NASA/CR--1998 207544

IN-35-CR
076317

Final Report • 4 March 1998

DC-8 SCANNING LIDAR CHARACTERIZATION OF AIRCRAFT CONTRAILS AND CIRRUS CLOUDS

Prepared by:

Edward E. Uthe, Principal Scientist
Norman B. Nielsen, Senior Research Engineer
Terje E. Oseberg, Systems Programmer
Applied Physical Sciences Laboratory

SRI Project 6555

Prepared for:

National Aeronautics and Space Administration
Ames Research Center
Moffett Field, California 94035-1000

Attn: Ms. E. P. Condon
Earth System Science Division, 239-20

Cooperative Agreement NCC 2-885

Approved:

Elizabeth J. Brackmann, Co-Director
Applied Physical Sciences Laboratory

CONTENTS

LIST OF ILLUSTRATIONS

LIST OF TABLES

SUMMARY

An angular-scanning large-aperture (36 cm) backscatter lidar was developed and deployed on the NASA DC-8 research aircraft as part of the SUCCESS (Subsonic Aircraft: Contrail and Cloud Effects Special Study) program. The lidar viewing direction could be scanned continuously during aircraft flight from vertically upward to forward to vertically downward, or the viewing could be at fixed angles. Real-time pictorial displays generated from the lidar signatures were broadcast on the DC-8 video network and used to locate clouds and contrails above, ahead of, and below the DC-8 to depict their spatial structure and to help select DC-8 altitudes for achieving optimum sampling by onboard in situ sensors. Several lidar receiver systems and real-time data displays were evaluated to help extend in situ data into vertical dimensions and to help establish possible lidar configurations and applications on future missions.

Digital lidar signatures were recorded on 8mm Exabyte tape and generated real-time displays were recorded on 8mm video tape. The digital records were transcribed in a common format to compact disks to facilitate data analysis and delivery to SUCCESS participants. Data selected from the real-time display video recordings were processed for publication-quality displays incorporating several standard lidar data corrections. Data examples are presented that illustrate (1) correlation with particulate, gas, and radiometric measurements made by onboard sensors, (2) discrimination and identification between contrails observed by onboard sensors, (3) high-altitude (13 km) scattering layer that exhibits greatly enhanced vertical backscatter relative to off-vertical backscatter, and (4) mapping of vertical distributions of individual precipitating ice crystals and their capture by cloud layers. An angular scan plotting program was developed that accounts for DC-8 pitch and velocity.

The DC-8 scanning lidar methodology and data examples were used to prepare an article (accepted for publication) for the SUCCESS special GRL issue, and to generate a web site (http://www.rsed.sri.com/ lidar) linked to the SUCCESS home page.

1 INTRODUCTION AND OBJECTIVES

The environmental consequences of subsonic and supersonic aircraft fleets need better definition for input to the design of future aircraft and their operational scenarios. NASA is developing a capability to predict the effects of current and future aircraft on the environment through use of a 3-D model. This model consists of modular parameterizations of effluent emissions and their microphysical and chemical transformations, dynamic behavior, and radiation budget perturbations. Experimental data are needed to better understand relevant atmospheric processes, to develop quantitative relationships that improve model performance, and to validate model predictions. Model simulations will be used to assess and report the effect of aviation on the environment.

As part of Atmospheric Effects of Aviation Project (AEAP), NASA formulated an extensive multi-aircraft field program, termed the Subsonic Aircraft: Contrail and Cloud Effects Special Study (SUCCESS), to characterize exhaust of aircraft in flight, to investigate aircraft exhaust impact on cirrus formation processes and radiation budgets, and to develop new instrumentation for use on future field studies. The SUCCESS field program was based from Salina, Kansas, primarily to take advantage of the available atmospheric measurements made at the Atmospheric Radiation Measurements (ARM) Clouds and Radiation Testbed (CART) site located in northern Oklahoma and southern Kansas.

Development of an angular scanning aerosol backscatter lidar installation on the NASA DC-8 research aircraft and its participation in the SUCCESS field experiments was funded by the AEAP program. The proposed lidar would be able to do an angular scan from vertically downward to vertically upward, and therefore be able to detect and measure cloud layers and contrails above, ahead of, and below the DC-8, as illustrated in Figure 1. Lidar range-resolved backscatter signatures would be processed and displayed in pictorial format in real time on the DC-8 video network so that the flight director, flight crew, and other experimenters would have information to position the aircraft and operate onboard in situ sensors to best sample contrails and clouds. The data would be recorded so that the lidar presentations could be used to extend measurements made along the flight path into vertical dimensions.

The proposed objectives of the lidar program are listed below:

- Map contrail/cloud distributions above and below the DC-8 to help establish best in situ sampling altitudes
- At sampling altitudes, map contrail/cloud vertical distributions ahead of the DC-8
- Provide data for establishing DC-8 in situ sensor sampling paths relative to vertical cloud/contrail distributions

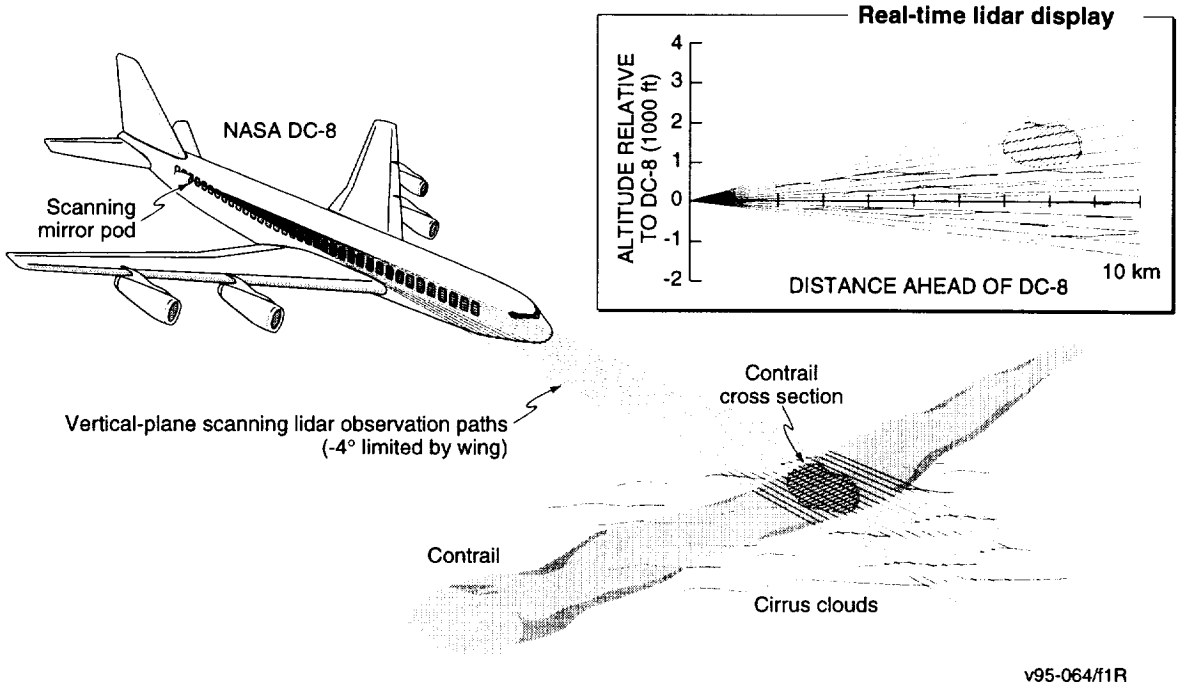

Figure 1 DC-8 SCANNING LIDAR ILLUSTRATION

- Analyze contrail/cloud radiative properties with combined lidar/radiometric measurements
- Evaluate aerosol mean particle sizes from two-wavelength (1.06 and 0.53 μm) lidar observations
- Study contrail/cloud interactions, diffusion, and mass decay/growth
- Provide a scanning mirror capability for other remote sensing instrumentation.

In this report, the lidar design is discussed in Section 2, and the lidar SUCCESS operations is discussed in Section 3. Section 4 presents several interesting data examples, and Section 5 presents conclusions and recommendations.

2 DC-8 LIDAR DESIGN

2.1 SCANNING MIRROR SYSTEM

The DC-8 angular scanning lidar development was predicated upon use of an existing ground-based scanning lidar with most of the development effort directed to the DC-8 scanning mirror system. Basically, a scanning mirror pod was envisioned to consist of a rotating cylinder containing a 45° optical mirror with an optical window mounted on the cylinder face. The mirror would redirect the laser transmitter path and coaligned receiver field of view from inside the aircraft through an aircraft window port to designated angles in a vertical plane oriented in the direction of aircraft travel. The system was to accommodate a telescope receiver aperture of 36 cm (14 inches) facilitated by the relatively large windows of the DC-8 aircraft.

A design study was conducted at NASA Ames using a preliminary scanning mirror concept and optical specifications provided by SRI. The design study identified the structural, aerodynamic, and system requirements to balance the performance needs of the lidar, while ensuring the scanner pod to be airworthy. Because in situ sampling ports needed installation in the front sections of the DC-8, the lidar scanner was designed for installation in the rear section of the aircraft and makes use of one of the DC-8's side-viewing window ports. In addition, the forward pointing direction was offset a few degrees from the flight direction so that the laser pulses would clear the air sampling probes protruding from the aircraft fuselage.

A pressurized scanner pod was developed that consists of a large, flat 45° diagonal mirror and an optical window mounted on a bearing assembly that is installed outside the aircraft in a cylindrical configuration, as illustrated in Figure 2. Pressurization at the pod surfaces eliminates the need for a window at the DC-8 fuselage surface and reduces the total number of optical surfaces interacting with laser pulses. The pod is motor driven and computer controlled for positioning or scanning. It can be used in either a forward, upward, or downward viewing configuration. The pod can be locked into any desired position with a pair of opposing cam clamps. Adjustable mechanical stops limit scanning of the pod from intersecting the wing area of the aircraft. An indexed template marked in degrees indicates the pointing position of the scanner. A fairing (Figure 3) was designed by NASA aerodynamicists to provide a smooth air flow around the scanner pod. The fairing is mounted to the side of the aircraft behind the scanner using two unused window ports to provide the attachment mounting support. Installation of the scanner pod and aerodynamic fairing on the DC-8 is pictured in Figure 4.

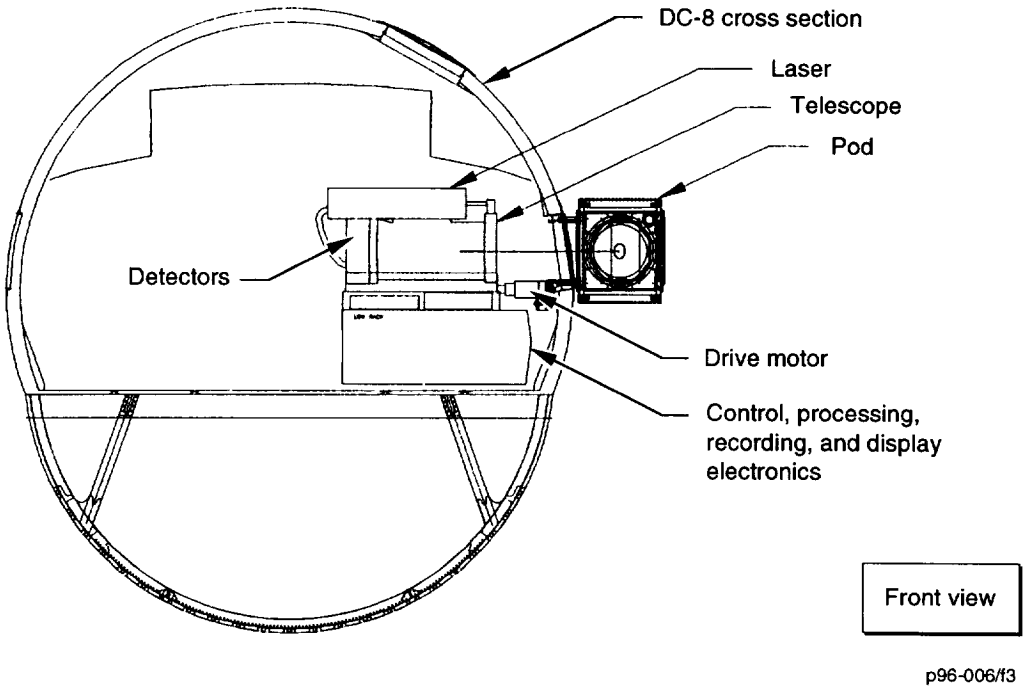

Figure 2 SRI SCANNING LIDAR INSTALLATION NASA AMES DC-8

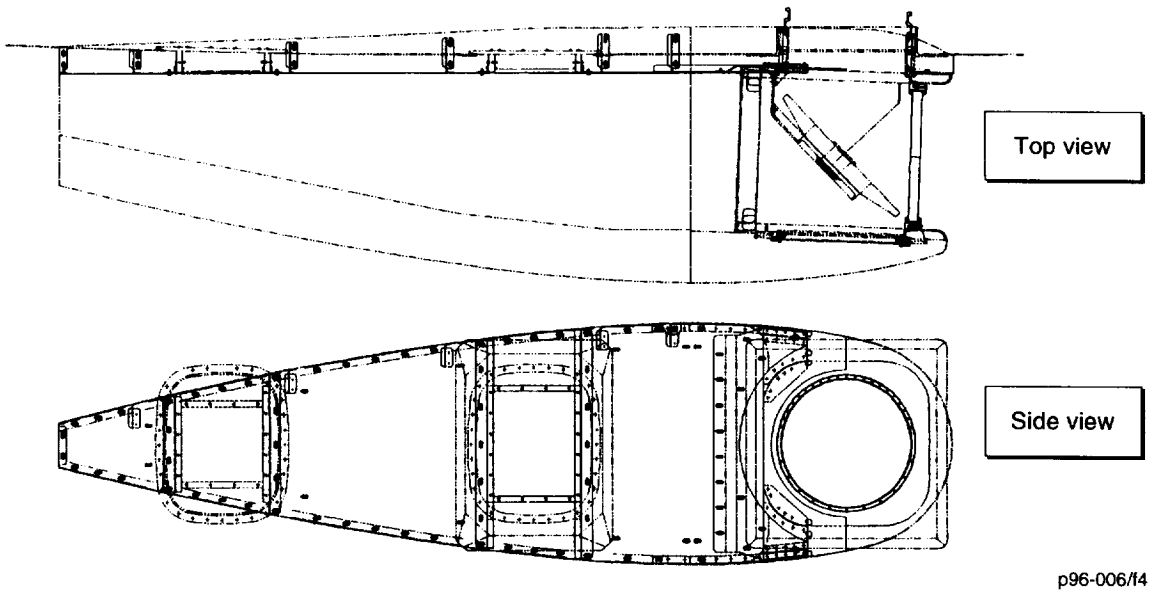

Figure 3 DC-8 LIDAR SCANNING MIRROR POD AND AERODYNAMIC FAIRING

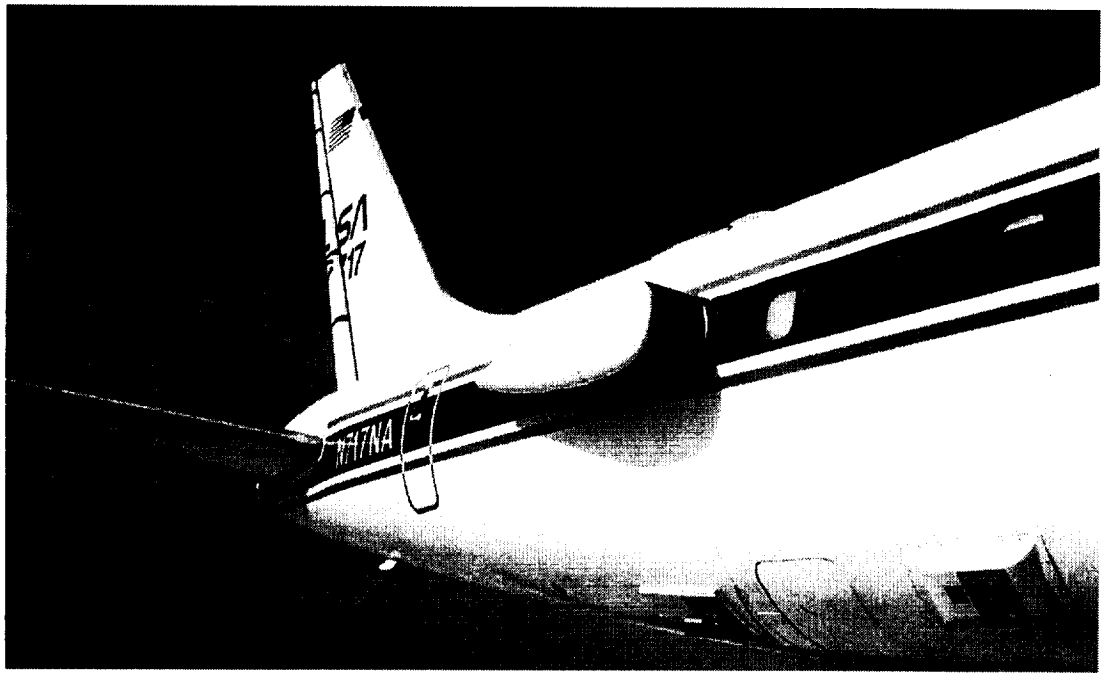

v97-056/f2-2/98

Figure 4 DC-8 SCANNING LIDAR POD AND AERODYNAMIC FAIRING INSTALLATION WITH POD POSITIONED FOR FORWARD LIDAR VIEWING

The scanner provides a 35 cm aperture for the lidar telescope receiver and will accommodate other SRI lidar systems. The front surface diagonal mirror was designed to be 1/8 wave flat. This helps maintain the astronomical quality of the telescope and allows focusing of backscattered light onto millimeter-size diameter optical detectors. In the center of the large diagonal mirror is an additional laser transmitter mirror that allows the lidar to be operated in a coaxial configuration. The high-energy transmitter mirror is 2 inches in diameter and can be changed to accommodate other wavelength lidar systems. The pressurized optical window of the pod (following the 45° mirror) is made of BK-7 glass, 17 inches in diameter and 1-1/4 inches thick. It has a high-energy antireflection coating on both surfaces to aid transmission and minimize energy reflection into the telescope. During landing and takeoff the scanner pod window is pointed in the aft-facing direction into the fairing for protection and for receiver calibration against a low-light-level background.

SRI provided the scanning mirror, optical window, drive motor, gear box, motor control, and computer interface to the scanning mirror system. The rotating pod and aerodynamic fairing constructed by NASA will remain a DC-8 asset for use on other projects.

2.2 LIDAR SYSTEM

The DC-8 angular scanning lidar employed the SRI Mark IX ground-mobile scanning lidar system with components repackaged to meet DC-8 installation requirements. The lidar has been updated several times including incorporating a 14-inch telescope and receiver system originally used on the ALPHA-1 airborne lidar flown in a fixed downward viewing direction on the SRI Queen Air aircraft. A Spectra Physics DCR-11 Nd:YAG laser system was also added. The laser transmitter, telescope receiver, scanning/fairing control unit, and data acquisition system were integrated into a standard DC-8 equipment rack provided by NASA.

A lidar block diagram is illustrated in Figure 5. The laser is a Spectra Physics model DCR-11 Nd:YAG with a second harmonic frequency doubler. The laser runs at 10 Hz with approximately 130 mJ at both of the two wavelengths (1064 nm and 532 nm). The laser power supply and heat exchanger are contained in a separate package mounted directly to the seat rails. The flash lamp and Q-switch trigger pulses are supplied from a custom lidar program control unit. The pulses are synchronized to 60 Hz line frequency to avoid possible ground loop interferences.

The lidar telescope has a 35 cm aperture with a Cassegrain configuration. Backscattered light from atmospheric aerosols is collected by the telescope and divided into two channels with a dichoric beam splitter. After passing through narrowband interference filters to reduce background light levels, the light from each channel is focused onto a solid state detector. On Channel 1 the 1064 nm detector (3 mm diameter) is enhanced for this wavelength and used in combination with a 60 dB logarithmic amplifier to obtain a large operating dynamic range. Data collected on this channel is primarily for short-range observation while flying directly through cirrus clouds and aircraft contrails. Channel 2 can be used for either the 1064 nm or 532 nm wavelength depending on receiver optical elements. The percentage of energy in each channel can be controlled by the beam splitter. The detector on Channel 2 is smaller in size (0.8 mm) and has more gain and radiant reponsitivity. This high sensitivity channel uses a 40 dB logarithmic amplifier and is used for long-range observation of subvisible clouds. In addition to the data from the two logarithmic channels, linear data from each channel can be digitized and recorded. For special experiments a polarizer can be added to the 1064 nm channel to differentiate between the crystal structure of cirrus clouds and aircraft contrails.

The lidar data acquisition system is based on an IBM PC. Up to four channels of data can be processed, using Gage Applied Sciences digitizers, and recorded on Exabyte tape. The two linear channels use 12-bit 30 MHz digitizers and the two logarithmic amplifier channels use 8-bit 50 MHz digitizers. A low-speed 8-channel 12-bit A-D card is available for processing signals from associated meteorological sensors such as a narrow-beam radiometer. The DC-8 aircraft flight parameters and related environmental data available on a NASA supplied data network is input to the lidar data system for recording and presentation on the lidar displays.

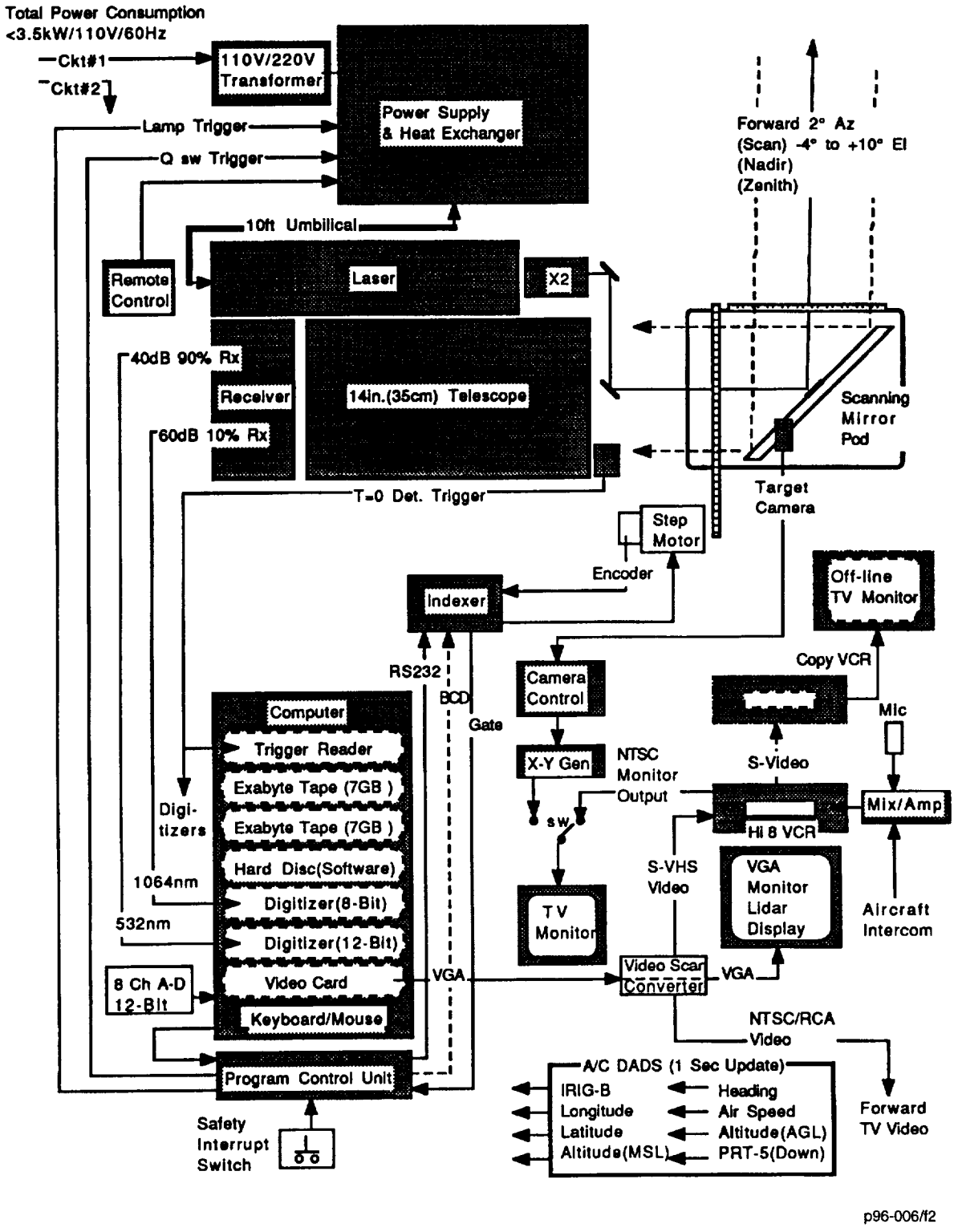

Figure 5 SRI DC-8 LIDAR CONFIGURATION (component block diagram)

A program control unit controls the stepping motor drive of the scanning mirror, and synchronizes it with the laser firing and data acquisition. The motor position is read by the lidar computer and added to the recorded data array. The lidar data are processed and displayed as color modulated pictorial displays in real time, on a flat panel VGA color monitor. The video signal passes through a scan converter and is input to the DC-8 video network so that contrail and cloud distribution displays are available to the mission manager, flight crew, and other experimenters for operational use. The video is also recorded on a HI-8 VCR (> 400 line resolution) so that it may be analyzed on standard television receivers.

3 SUCCESS FIELD OPERATIONS AND DATA SUMMARIES

SRI submitted to NASA a DC-8 integration questionnaire (Appendix A) and an airborne lidar experiment plan (Appendix B). The experiment plan provided information on lidar operational procedures, potential hazards, and safeguards—mostly addressing eye safety considerations. The plan was approved with the stipulation that SRI be responsible for safe operation of the lidar during approved operational times and constraints dictated by the mission manager.

No ground testing of the lidar was permitted, therefore, the first opportunity to test the system was during the test flight conducted on 10 April 1996. The lidar operated relatively well except for real-time video displays. The scanning lidar was able to detect and map DC-8 generated contrails to a distance of 14 km (Figure 6). The DC-8 aircraft log states that NO was detected by the in situ instrumentation at 00:51:03 GMT in good agreement with the time of aircraft penetration of the contrail observed by the lidar.

The second test flight, conducted on 13 April 1996, also served to transport the aircraft from Ames Research Center to Salina, Kansas. Fifteen data collection flights originated from Salina from 15 April through 10 May. The 10 May flight also provided transport and re-establishment of operations at Ames Research Center. Two additional research flights were made from Ames on 12 and 15 May to provide observations over the waters of the Pacific Ocean. A condensed log of lidar operational times, angular scan mode, and contrail/cloud observation remarks is given in Table 1. Table 2 presents additional information on lidar configurations and data tape inventory for each SUCCESS flight day. Table 3 lists the digitization range resolution and maximum range for each of the four lidar backscatter signature channels.

The lidar was normally operated at vertical up or down viewing angles to establish the presence and altitude of cloud and/or contrails above and below the aircraft. At sampling altitudes the lidar was normally operated in forward viewing angular scan patterns to map the vertical structure of clouds and contrails ahead of and penetrated by the aircraft. However, eye safety constraints sometimes prohibited lidar operation, or limited operation to only vertical viewing directions.

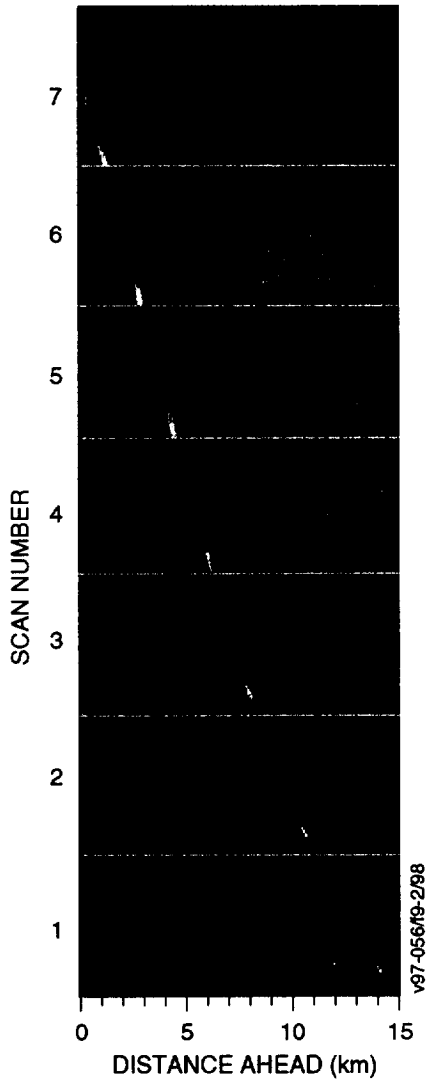

Figure 6 **DC-8 LIDAR FORWARD-VIEWING SCAN OBSERVATIONS AS THE AIRCRAFT APPROACHES A CONTRAIL GENERATED EARLIER BY THE DC-8. Data are plotted with a vertical axis of time (scan angle) and a horizontal axis of distance ahead of the DC-8. 11 April 1996, 00:49:21 to 00:50:50 GMT.**

Table 1

DC-8 SCANNING LIDAR SUCCESS OPERATIONS LOG SUMMARY

Time (GMT) Start	End	Scan[1] Angle (°)	Remarks
4/10/96			
2355	0053	–3, +5	IR on Ch1, green on Ch2/mapping of DC-8 contrail
4/13/96			
1803	1835	+90	Clouds and contrails above aircraft
1911	1929	–3, 5	Clouds above aircraft
4/15/96			
1754	1849	–90	Boundary layer clouds only/1.5 km AGL
4/16/96			
1742	1800	–3, 0	Aircraft approaching clouds
1800	1805	–3, 10	Clouds
1805	1906	–3, 0	Clouds
1917	1936	–3, 10	Aircraft approaching clouds
1936	1950	–3, 10	Mostly clear
1958	2002	–3, 10	Mostly clear/contrail
2008	2015	–3, 10	Mostly clear
2030	2048	–3, 5	IR on Ch1 and Ch2, mostly clouds above aircraft
2057	2105	–3, 2	Clouds penetrated by aircraft
4/18/96			
1731	1750	–3, 0	Clear
1750	1802	–3, 5	Clear
1808	1843	+90	Clear/T-39 ahead DC-8
1925	1932	–3, 5	Clear
1932	2024	–4, 5	Mostly clear/some clouds penetrated
4/20/96			
1547	1601	–4, 4	Mostly clear
1601	1625	0, 10	Cloud layer above aircraft
1625	1703	0, 8	Clouds above/cloud penetrations near 1700 Z
1750	1732	0, 10	Thin layer above
1736	1758	0, 10	Cloud penetrations
1758	1858	–4, 10	Cloud penetrations/5 Hz rate at 1852
1858	1920	0, 10	Cloud penetrations/5 Hz rate
1920	1922	0, 8	Cloud penetrations/5 Hz rate
1945	2024	0, 10	Back at 10 Hz/cloud penetrations
2025	2047	0	Map of clouds/contrails ahead of aircraft

[1] 90° vertically upward, 0° forward, and –90° vertically downward viewing.

Table 1

DC-8 SCANNING LIDAR SUCCESS OPERATIONS LOG SUMMARY (continued)

Time (GMT) Start	End	Scan[1] Angle (°)	Remarks
4/21/96			
1753	1815	–1, 9	Cloud layer above aircraft
1815	1822	–4, 10	Cloud penetrations
1822	1824	–1, 10	Cloud layer above aircraft
1824	1834	–4, 10	Cloud penetrations/denser above aircraft
1853	1902	–4, 10	Cloud layer above/penetrate cumulus tops
1912	*	–4, 8	DADS disconnected/DC-8 contrails
2051	2125	–4, 8	DADS on/cloud and contrails penetration
4/24/96			
1706	1712	–4, 1	Cloud penetration by aircraft
1712	1725	–4, 7	Cloud and contrail penetrations
1725	1726	–4, 4	
1732	1753	0, 10	Aircraft approaching and penetrating clouds
1828	1903	0, 5	Cloud and contrail penetrations
1903	1945	–1, 5	Cloud penetrations/some contrails?
2031	2055	+90	Cloud layer above aircraft/in cloud ~2052
2102	2115	0, 8	Cloud penetrations
2122	2133	–2, 6	Cloud penetrations by aircraft
2145	2157	0, 5	Cloud penetrations by aircraft
2201	2220	–90	Cloud layer extend to 2 km below aircraft
2225	2254	–3, 5	Cloud and contrail penetrations
2302	2324	0	Forward viewing cloud penetrations
4/27/96			
1644	1831	–4, 5	T-39 contrail penetrations
1831	1834	–4, 10	
1834	1855	–2, 10	Cloud penetrations
1856	1857	–4, 10	Cloud layer above aircraft
1857	1918	–4, 5	Mostly clear
1918	1937	–4, 10	Cloud penetrations/contrails?
1937	2016	–4, 5	Cloud top penetrations/DC-8 contrail
2027	2122	–4, 5	Mostly clear/some clouds
2122	2144	–4, 10	Cloud layer mostly above aircraft
2144	2145	–4, 8	Low density cloud penetrations
2145	2149	–4, 10	Low density cloud penetrations
2150	2156	+90	Thin cloud near aircraft
2156	2157	–4, 21	Wide sector scan/some cloud at aircraft altitude
2157	2214	–4, 10	Cloud penetrations

[1] 90° vertically upward, 0° forward, and –90° vertically downward viewing.

Table 1

DC-8 SCANNING LIDAR SUCCESS OPERATIONS LOG SUMMARY (continued)

Time (GMT) Start	End	Scan[1] Angle (°)	Remarks
4/29/96			
1923	1938	+90	Clear above aircraft
1939	1944	–4, 3	Clear ahead of aircraft
4/30/96			
1728	1747	–4, 4	Clear/contrail
1748	1804	–2, 0	Clear
1809	2314	+90	Clear with occasional widespread thin layers <3 km above aircraft/some layer penetrations
5/2/96			
1637	1740	+90	1637 layer 6 km above/1706 layer 0.5 km above/ 1717–1735 aircraft in layer
1805	1816	–90	Many stratified layers and contrails/convective cloud tops 3 km above surface
5/3/96			
1932	1946	–4, 4	Clear with 757 contrail returns
2023	2034	–4, 4	Clear with 757 contrail returns
2141	2229	–90	Mostly clear/haze layer near surface/layer 1–2 km below aircraft after 2204/layer penetration 2227
5/4/96			
1733	1737	+90	IR only Ch1/clear
1737	1749	+90	Green on/layer 3–4 km above/757 contrail cross sections
1858	2046	–4, 0	IR Ch1 and Ch 2/many 757 contrails/no clouds
2054	2136	–90	Mostly low clouds (2 km above sfc)/cloud layer 3 km below aircraft 2126–2131 and 2135
5/7/96			
1818	1821	+90	Contrail 1 km above/lidar shut down by flight operations over Denver space
5/8/96			
1719	1749	+90	IR Ch 1 and Ch 2/layer 4–5 km above at start/ penetration of layer near 1727/clear above after 1735
1749	1823	–90	Clear except clouds near surface
1823	1841	+90	Cloud layer extending to about 1 km above aircraft
1845	1931	+90	Clear
1931	2005	+90	Cloud layer just below aircraft/cloud layer penetration near 1940/clear after 1942

[1] 90° vertically upward, 0° forward, and –90° vertically downward viewing.

Table 1

DC-8 SCANNING LIDAR SUCCESS OPERATIONS LOG SUMMARY (concluded)

Time (GMT) Start	End	Scan[1] Angle (°)	Remarks
5/8/96			
2005	2045	+90	Cloud layer extending to about 1 km above/clear after 2041
2046	2053	–90	Cloud layer near surface/layer 1 km below at 2050/ possible penetration of layer 2052
5/10/96			
1436	1644	+90	IR Ch1 and 2/data gaps during aircraft turns/ widespread 43,000 ft layer/layer return greatly decreases with nonzenith viewing indicating ice crystals
5/12/96			
2018	2055	+90	IR on Ch1 and Ch 2/mostly clear above aircraft/some thin layers (contrails?)
2250	2302	+90	Layer extending from aircraft upward to about 0.5 km
2313	2445	–90	Complex distributions of cloud, contrails, and precipitating ice crystals extending to about 3 km below aircraft/multiple DC-8 contrails from oval flight pattern/aircraft penetrations of cloud and contrails
5/15/97			
1948	2022	+90	IR on Ch 1 and Ch2/thin layer just below aircraft/appears aircraft penetrates layer
2023	2116	–90	Multiple layers/mostly dense layer (2 km thick) at varying distances (3 to 8 km) below aircraft (6 to 8 km above surface)
2205	2248	+90	Mostly clear above aircraft/some cloud patches near (at) aircraft altitude
2248	2255	+90	Layer from aircraft to 1 km above
2255	2301	+90	Clear above aircraft
2301	2321	+90	Layer within 1 km above aircraft
2321	2323	+90	Clear above aircraft
2331	2400	–90	Multiple very thin layers/dense layer begins 2342 2 km below aircraft/cloud penetration 2358 to about 2400 GMT

[1] 90° vertically upward, 0° forward, and –90° vertically downward viewing.

Table 2
DC-8 SCANNING LIDAR SUCCESS CONFIGURATION AND DATA INVENTORY SUMMARY

DATE 1996	DAY	FLIGHT	TAPE INVENTORY NASA VIDEO[1]	TAPE INVENTORY SRI VIDEO[2]	TAPE INVENTORY SRI DATA[3]	RECEIVER BEAMSPLITTER 60 dB/40 dB	RECEIVER WAVELENGTH 60 dB/40 dB	DATA COLLECTION PROGRAM	REMARKS
4/10	101	960201	0	1	2	10%/90%	IR/G	GO1	G and IR radar plots: fixed angle vertical in km, horizontal in time/scan vertical in 1000 ft, horizontal in time.
4/13	104	960202	1	1	3	10%/90%	IR/G	GO1	
4/15	106	960203	1	1	1	10%/90%	IR/G	GO1	
4/16	107	960204	1	2	3	10%/90%	IR/G, IR/IR	GO1	IR/IR > 2030 GMT.
4/18	109	960205	1	1	2	10%/90%	IR/G	GO1	
4/20	111	960206	1	3	6	Dichroic	IR/G	G01	5 Hz lidar rate tested (1352–1426 Z).
4/21	112	960207	2	1	10	Dichroic	IR/G	GO3/GO2	GO3 and GO2 did not fix computer problem GO3 introduced missed shots problem/DADS not recorded on some data.
4/24	115	960208	2	3	8	Dichroic	IR/G	GO3	
4/27	118	960209	2	3	1	Dichroic	IR/G	GO16	New IR receiver installed/computer failure problem fixed. New plots 5000 ft interval A-scope, 5000 ft interval fixed angle.
4/29	120	960210	2	3	1	Dichroic	IR/G	GO17	Varied dB/V on plots.
4/30	121	960211	2	2	3	Dichroic	IR/G	GO17	Adjusted G (40 dB) detector gains. Changed recording ranges requiring tape changes.
5/2	123	960212	2	1	1	Dichroic	IR/G	GO17	
5/3	124	960213	1	2	1	Dichroic	IR/G, IR/IR	GO17	
5/4	125	960214	1	2	1	10%/90%	IR/IR, IR/G	GO17	IR/IR to 1737 Z, IR/G to 1858 Z, IR/IR.
5/7	128	960215	1	0	1	10%/90%	IR/IR	GO17	Only few minutes of operation allowed.
5/8	129	960216	1	2	1	10%/90%	IR/IR	GO17	Receiver calibration.
5/10	131	960217	1	1	1	10%/90%	IR/IR	GO17	Changed grayscale setting to better view high-altitude layer (above DC-8 ceiling).
5/12	133	960218	1	2	1	10%/90%	IR/IR	GO17	
5/15	136	960219	1	2	1	10%/90%	IR/IR	GO17	Adjusted 40 dB detector gains depending on signal strength.

[1]VCR/VHS [2]VCR/HI-8 mm [3]8 mm Exabyte

Table 3

DC-8 SCANNING LIDAR DATA DIGITIZATION SUMMARY

SUCCESS PROJECT (NASA) DATA COLLECTION SUMMARY														
			Number of Points/Shot				Sample Interval (ns)				Range (km)			
Date	File Base Name	Tape Number	IR-LOG	GREEN-LOG	IR-LINEAR	GREEN-LINEAR	IR-LOG	GREEN-LOG	IR-LINEAR	GREEN-LINEAR	IR-LOG	GREEN-LOG	IR-LINEAR	GREEN-LINEAR
10-Apr-96	96101	1	5000	5000	808	808	20	20	33	33	15	15	4	4
		2	5000	5000	808	808	20	20	33	33	15	15	4	4
13-Apr-96	96104	1	5000	5000	606	606	20	20	33	33	15	15	3	3
		2	5000	5000	606	606	20	20	33	33	15	15	3	3
		3												
15-Apr-96	96106	1	3333	3333	202	202	20	20	33	33	10	10	1	1
16-Apr-96	96107	1	5000	5000	1010	1010	20	20	33	33	15	15	5	5
		2	5000	5000	1010	1010	20	20	33	33	15	15	5	5
		3	5000	5000	1010	1010	20	20	33	33	15	15	5	5
18-Apr-96	96109	1	5000	5000	1010	1010	20	20	33	33	15	15	5	5
		2	5000	5000	1010	1010	20	20	33	33	15	15	5	5
20-Apr-96	96111	1	5000	5000	3030	1010	20	20	33	33	15	15	15	5
		2	5000	5000	2020	202	20	20	33	33	15	15	10	1
		3	5000	5000	2020	202	20	20	33	33	15	15	10	1
		4	5000	5000	1010	202	20	20	33	33	15	15	5	1
		5	5000	5000	1010	202	20	20	33	33	15	15	5	1
		6	4333	4333	404	202	20	20	33	33	13	13	2	1
21-Apr-96	96112	1	5000	5000	1010	202	20	20	33	33	15	15	5	1
		2	5000	5000	1010	202	20	20	33	33	15	15	5	1
		3	5000	5000	1010	202	20	20	33	33	15	15	5	1
		4	5000	5000	1010	202	20	20	33	33	15	15	5	1
		5	5000	5000	1010	202	20	20	33	33	15	15	5	1
		6	5000	5000	1010	202	20	20	33	33	15	15	5	1
		7	5000	5000	1010	202	20	20	33	33	15	15	5	1
		8	6666	6666	1212	1212	20	20	33	33	20	20	6	6
		9	6666	6666	1212	1212	20	20	33	33	20	20	6	6
		10	5000	5000	1010	202	20	20	33	33	15	15	5	1
24-Apr-96	96115	1	5000	5000	4	4	20	20	6700	6700	15	15	4	4
		2	5000	5000	4	4	20	20	6700	6700	15	15	4	4
		3	5000	5000	4	4	20	20	6700	6700	15	15	4	4
		4	5000	5000	4	4	20	20	6700	6700	15	15	4	4
		5	5000	5000	4	4	20	20	6700	6700	15	15	4	4
		6	5000	5000	4	4	20	20	6700	6700	15	15	4	4
		7	5000	5000	4	4	20	20	6700	6700	15	15	4	4

Table 3

DC-8 SCANNING LIDAR DATA DIGITIZATION SUMMARY
(concluded)

SUCCESS PROJECT (NASA) DATA COLLECTION SUMMARY

			Number of Points/Shot				Sample Interval (ns)				Range (km)			
Date	File Base Name	Tape Number	IR-LOG	GREEN-LOG	IR-LINEAR	GREEN-LINEAR	IR-LOG	GREEN-LOG	IR-LINEAR	GREEN-LINEAR	IR-LOG	GREEN-LOG	IR-LINEAR	GREEN-LINEAR
		8	5000	5000	4	4	20	20	6700	6700	15	15	4	4
27-Apr-96	96118	1	5000	5000	2352		20	20	17		15	15	8	
29-Apr-96	96120	1	1333	1333	1568		20	20	17		4	4	4	
30-Apr-96	96121	1	11766	11766	492		20	20	17		35	35	1	
		2	6666	6666	492		20	20	17		20	20	1	
		3	3333	3333	1960		20	20	17		10	10	5	
2-May-96	96123	1	3333	3333	4021		20	20	17		10	10	10	
3-May-96	96124	1	5333	5333	6274		20	20	17		16	16	16	
4-May-96	96125	1	5000	5000	5882		20	20	17		15	15	15	
7-May-96	96128	1	5000	5000	5882		20	20	17		15	15	15	
8-May-96	96129	1	5000	5000	5882		20	20	17		15	15	15	
10-May-96	96131	1	5000	5000	5882		20	20	17		15	15	15	
12-May-96	96133	1	5000	5000	5882		20	20	17		15	15	15	
15-May-96	96136	1	5000	5000	5882		20	20	17		15	15	15	
Totals														

Lidar backscatter signatures were digitized and computer processed in real time in terms of two-dimensional intensity-modulated pictorial displays depicting the structure of observed clouds and contrails. The fixed angle observations were displayed with time and range axes and the angular scan observations were displayed in a polar scan format with altitude and horizontal distance axes. The real-time display was scan converted to standard NTSC (TV) video format and input to the DC-8 video network so that the display could be viewed throughout the aircraft and used by the flight director to help establish aircraft sampling altitudes. Because the polar scan format does not provide good presentation of scattering features near the aircraft (e.g., in the apex of the scan), some angular scan data were displayed in a nonpolar format. However, it was determined that the polar scan was the best display for interpreting targets at long ranges from the aircraft and signal return as a function of range for interpreting targets at short ranges from the aircraft. Examples of the real-time display of angular scan data that evolved during the flight program are shown in Figure 7. The backscatter signature for each lidar observation was displayed as the lidar was scanned and the polar scan display was generated. The pitch angle of the aircraft supplied by the DC-8 data network was incorporated into the real-time displays to provide true viewing angles.

The laser was fired at a rate of 10 Hz and the scanning mirror was rotated at 1° per second. The starting, ending, and incremental angles as well as the scan rate were computer controlled and easily adjusted by thumb switches on the lidar program unit.

Following the SUCCESS field program, the lidar data records were transcribed to compact disks (CDs) in a common format to facilitate data transfer to SUCCESS participants and for data analyses. This reduces complications of data use because of hardware and software changes made during the field program. Table 4 lists the lidar database that resides on 37 CDs. The file name contains the date of data collection. Operational times are derived from the DC-8 data network (DADS) and, therefore, missing times listed in Table 4 indicate that the lidar system was not connected to the network.

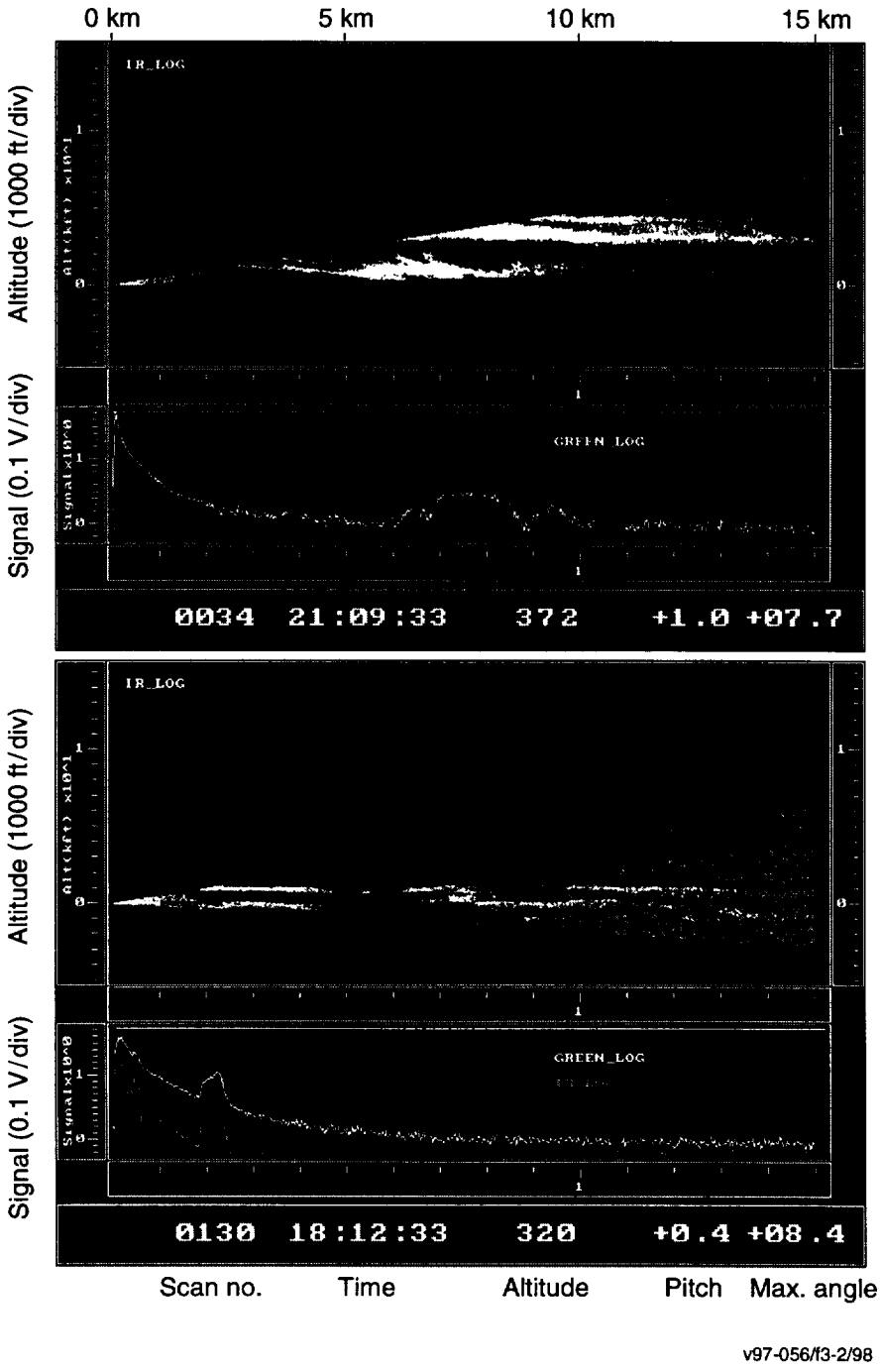

Figure 7 REAL-TIME ANGULAR SCAN VIDEO DISPLAYS GENERATED BY THE DC-8 SCANNING LIDAR SYSTEM

Table 4

DC-8 SCANNING LIDAR COMPACT DISK DATABASE SUMMARY

DISK NO.	FILE NAME	START TIME	END TIME
1	96041001.dat	23:55:06	00:52:36
	96041002.dat	23:21:37	23:22:37
	96041301.dat	18:03:29	18:33:52
	96041302.dat	19:11:30	19:36:41
2	96041501.dat	17:53:52	18:48:44
	96041601.dat	17:42:29	19:08:13
	96041602.dat	19:17:04	20:03:27
	96041603.dat	20:08:40	21:04:49
3	96041801.dat	17:30:43	19:40:01
	96041802.dat	19:47:58	20:24:01
4	96042001.dat	: :	16:47:33
5	96042002.dat	16:47:33	17:02:53
	96042003.dat	17:29:25	17:32:46
	96042004.dat	17:36:45	18:23:22
	96042005.dat	18:52:24	19:22:08
	96042006.dat	19:45:15	20:46:39
6	96042007.dat	18:28:06	18:47:53
	96042101.dat	17:53:49	18:31:58
	96042102.dat	18:48:38	18:49:06
	96042103.dat	18:53:04	19:01:11
	96042104.dat	: :	: :
	96042105.dat	: :	: :
	96042106.dat	: :	: :
	96042107.dat	: :	: :
7	96042108.dat	0:51:08	21:03:21
	96042109.dat	20:51:08	21:03:21
	96042110.dat	21:09:00	22:32:54
	96042401.dat	17:06:14	17:33:59
	96042402.dat	17:38:24	18:50:27
	96042403.dat	18:54:22	19:30:44
	96042404.dat	19:38:46	19:45:27
	96042405.dat	19:50:24	20:55:58
	96042406.dat	21:02:23	22:06:35
8	96042407.dat	22:12:18	22:30:13
	96042408.dat	22:34:35	23:24:34
	96042701.dat	16:43:59	18:34:05

Table 4

DC-8 SCANNING LIDAR COMPACT DISK DATABASE SUMMARY (continued)

DISK NO.	FILE NAME	START TIME	END TIME
9	96042702.dat	18:34:06	20:56:59
10	96042703.dat	20:56:59	22:14:02
	96042901.dat	19:23:30	19:44:36
	96043002.dat	18:09:01	18:25:36
11	96043001.dat	17:24:48	18:03:55
12	96043003.dat	18:25:36	19:02:59
13	96043004.dat	19:07:44	23:14:20
	96050201.dat	16:37:25	16:54:00
14	96050202.dat	16:54:00	18:16:14
	96050301.dat	19:31:41	20:29:35
15	96050302.dat	20:29:35	22:08:55
16	96050303.dat	22:08:55	22:29:09
	96050401.dat	17:33:12	17:44:55
17	96050402.dat	17:44:55	19:48:48
18	96050403.dat	19:48:48	20:58:37
19	96050404.dat	20:58:37	21:33:50
20	96050405.dat	21:33:50	21:35:48
	96050801.dat	17:19:02	17:53:02
21	96050802.dat	17:53:02	18:29:36
22	96050803.dat	18:29:36	19:06:59
23	6050804.dat	19:06:59	19:49:22
24	96050805.dat	19:49:22	20:24:02

Table 4

DC-8 SCANNING LIDAR COMPACT DISK DATABASE SUMMARY (concluded)

DISK NO.	FILE NAME	START TIME	END TIME
25	96050806.dat	20:24:02	20:53:17
	96050701.dat	18:18:37	18:20:39
26	96051001.dat	14:37:40	15:19:52
27	96051002.dat	15:19:52	16:12:58
28	96051003.dat	16:12:58	16:43:58
	96051501.dat	19:48:11	20:08:29
29	96051201.dat	20:18:02	23:14:37
30	96051202.dat	23:14:37	23:48:29
31	96051203.dat	23:48:29	0:21:39
32	96051204.dat	0:21:39	0:45:31
33	96051502.dat	20:08:29	20:47:17
34	96051503.dat	20:47:17	22:31:05
35	96051504.dat	22:31:06	23:23:09
36	96051505.dat	23:23:09	23:57:12
37	96051506.dat	3:26:28	0:00:28

4 DATA ANALYSIS EXAMPLES

Forward looking angular scan displays provided information on the vertical distribution of clouds and contrails ahead of the DC-8. However, several problems confront this mode of operation and data display. The display is distorted because of aircraft travel during the angular scan. For a 10° sector, the aircraft normally travels about 2 km between the first and last lidar observation of the scan. Moreover, when the DC-8 trailed behind another aircraft as a means to sample its emissions, wake vortices generated by the test aircraft introduced erratic DC-8 motions that translated into lidar pointing jitters so that cloud and contrail targets could not be uniformly scanned. A computer program is being developed to at least partially correct for aircraft travel and erratic motions. The data examples presented below were developed from fixed viewing angle observations.

During 12 May 1996, the DC-8 sampled its own contrail by flying a series of oval-shaped orbits. During the second orbit the DC-8 repeatedly penetrated the contrail generated during the first orbit by increasing and decreasing its altitude in a sinusoidal pattern. Figure 8 presents DC-8 lidar data collected with a fixed downward viewing direction and shows the contrail just below the DC-8 at times the DC-8 was above the contrail with other aerosol layers below. Above the lidar data display are plotted corresponding time histories of liquid water content, NO_y gas concentration, radiometric infrared (IR) blackbody temperature (narrow-beam downward-pointing radiometer), and upwelling solar flux (relative units) as measured by onboard sensors and supplied by other experimenters (see Section 6, Acknowledgments). The lidar display clearly depicts times when the contrail is below the aircraft and indicates times when the aircraft penetrated the contrail. These times agree well with times of observed increased water content and NO_y concentrations. The combined lidar and in situ observations establish times the contrail was above the aircraft as indicated in Figure 8. The radiometric data agree with this analysis showing cooler IR temperature and increased upwelling solar flux at times when the contrail was below the aircraft. Although the solar radiometric data have not yet been calibrated or corrected for aircraft motions, it appears that the albedo is increased by about 30% by the presence of the contrail.

Figure 9 presents data collected several minutes after that of Figure 8. The NO_y data again indicate that the scattering feature observed directly below the DC-8 resulted from aircraft emissions. Times when the lidar indicates contrail penetration by the DC-8 again agree with the time history of data collected from the onboard in situ and radiometric sensors. However, at 23:26:30 GMT the lidar observed two distinct contrails at different altitudes, with the first contrail sampled by the onboard sensors at 23:27:00 GMT and the second contrail sampled by the sensors at times after 23:27:10 GMT. It appears that the NO_y-to-water content ratio is

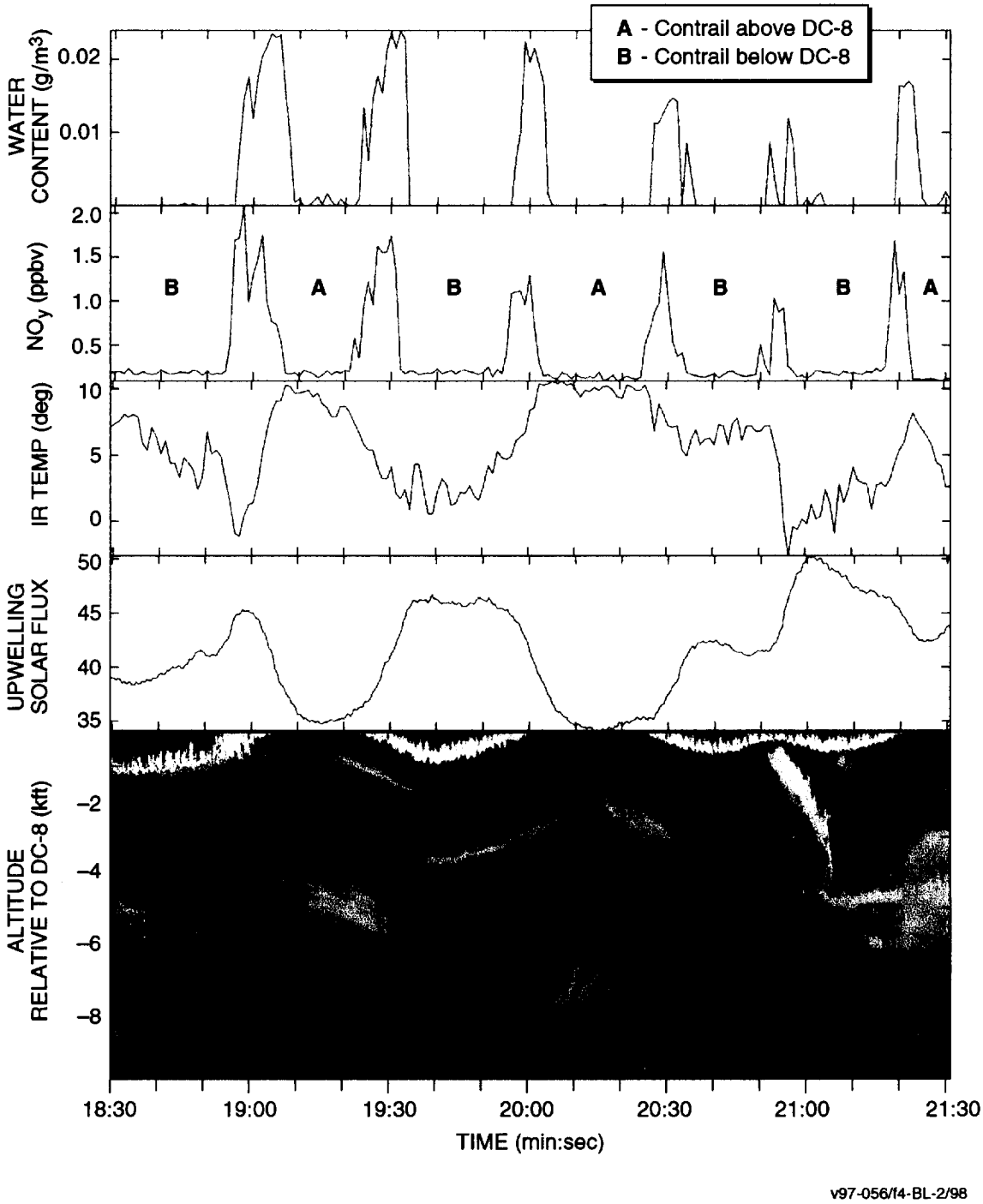

Figure 8 LIDAR AND SELECTED IN SITU AND RADIOMETRIC DATA AT TIMES OF THE DC-8 PENETRATING ITS EARLIER GENERATED CONTRAIL, 12 MAY 1996, 23:18:30 TO 23:21:30 GMT (DC-8 altitude approximately 36 kft)

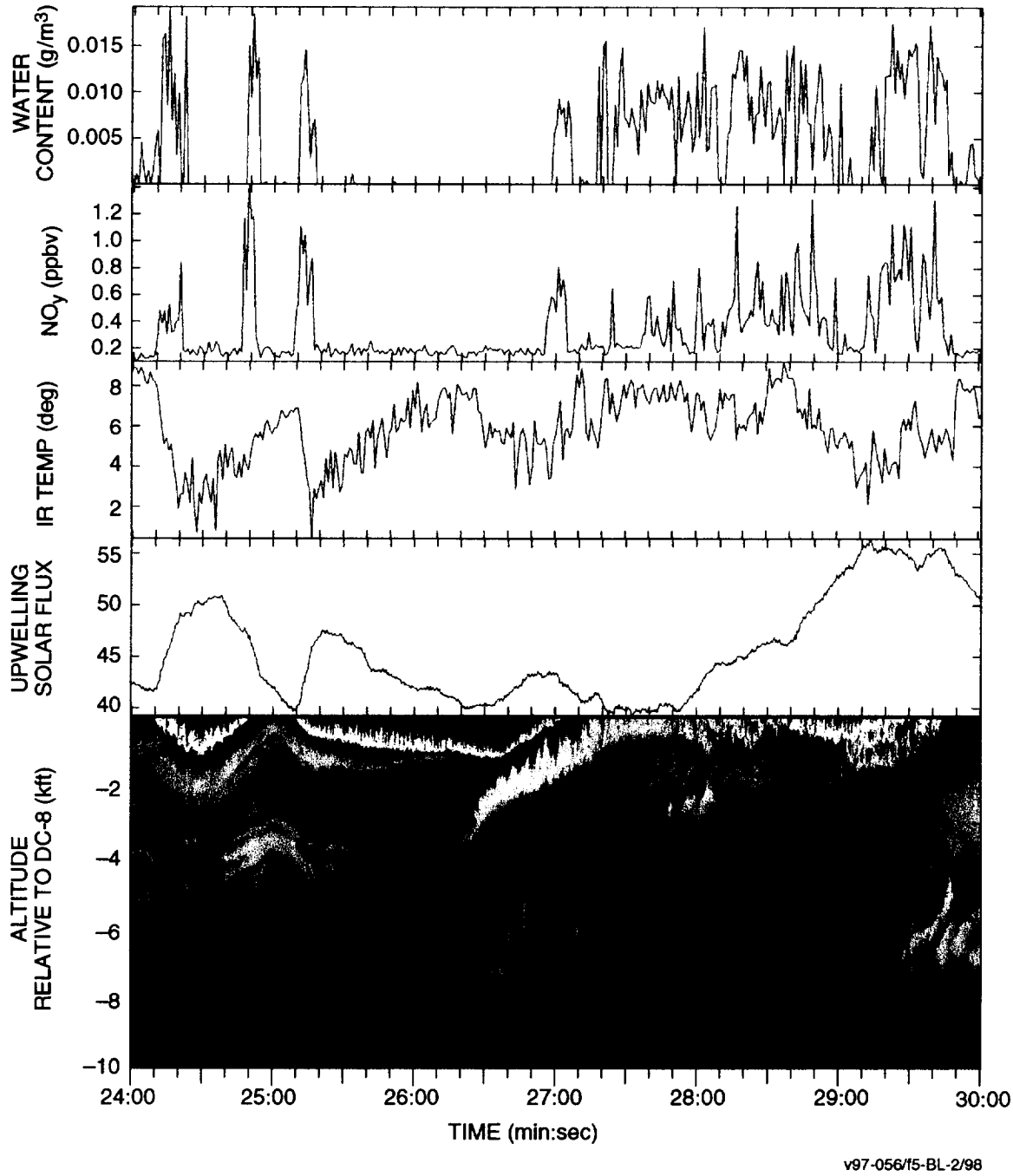

Figure 9 LIDAR AND SELECTED IN SITU AND RADIOMETRIC DATA AT TIMES OF THE DC-8 PENETRATING ITS EARLIER GENERATED CONTRAIL, 12 MAY 1996, 23:24:00 TO 23:30:00 GMT (DC-8 altitude approximately 36 kft)

smaller for the later sampled contrail. An analysis of the DC-8 flight paths indicates that the first sampled contrail resulted from the first DC-8 orbit and the later sampled contrail resulted from the second DC-8 orbit. Without the lidar data, this distinction between different aged contrails being sampled by the in situ sensors may have gone unnoticed.

On 10 May 1996, the lidar observed, over a large regional area, a thin scattering layer at an altitude of about 13.1 km (43,000 ft) MSL—above the flight ceiling of the DC-8 during this flight. Figure 10 presents upward viewing lidar returns from the layer before and after an aircraft turn that was made at an aircraft altitude of about 5.2 km (17,000 ft) MSL. The backscatter from the particulate layer sharply decreases as the aircraft turn is initiated and the laser pulses intersected the layer at nonvertical angles. This behavior has been observed by Uthe and Russell [1977] for high-altitude tropical cirrus consisting of horizontally aligned plate-shaped ice crystals, and has been observed by several other lidar researchers [Intrieri et al., 1995; Thomas et al., 1990]. The rate of backscatter decrease with angle is dependent on size, shape, and orientation of the crystals [Platt, 1978]. The scanning lidar provides a means to measure the zenith-enhanced backscatter without aircraft turns that affect other measurements such as solar and infrared flux. The horizontal alignment has been explained by falling crystals orienting themselves to offer maximum resistance to motion [Platt, 1978].

It may be possible to detect individual precipitating crystals with lidar—especially if horizontally aligned precipitating crystals are viewed by a vertically pointing lidar at relatively short ranges from the lidar before significant beam divergence occurs. Figure 11 presents vertically downward viewing lidar data collected on 12 May during a time period in which precipitating ice crystals were noted by other experimenters. The lidar plot shows many one-pixel strong returns (speckles) above the cloud located near 1.2 km (4,000 ft) below the DC-8 altitude of 11.9 km (39,000 ft) and no strong returns superimposed on the clear-air returns below the cloud indicating the crystals are completely scavenged by the cloud. Clear air returns below the cloud indicate that the absence of the speckles is not caused by cloud attenuation of the laser energy. The DC-8 contrail from an earlier orbit was located above the DC-8 and was probably the source of the precipitating crystals. The top of the cloud below the aircraft exhibits vertical striations possibly as a result of the influx of precipitating crystals.

The DC-8 scanning lidar can view in the direction of aircraft travel to remotely observe atmospheric volumes the aircraft is about to penetrate and be sampled by onboard in situ aerosol and gas sensors. Most of the forward viewing observations were conducted by scanning the lidar viewing over an angular sector as illustrated by Figure 1 as a means to generate data displays as shown by Figure 7; those observations provide information on the vertical structure of contrails and clouds sampled by the onboard sensors. However, Figure 12 presents a data example with the lidar viewing angle fixed forward in the aircraft flight direction. Onboard in situ sensor data collected at the time the remotely detected aerosol features are penetrated by the DC-8 verifies the scattering features as clouds or contrails. The airborne horizontal lidar viewing facilitates evaluation of atmospheric homogeneity and optical properties [Measures, 1984].

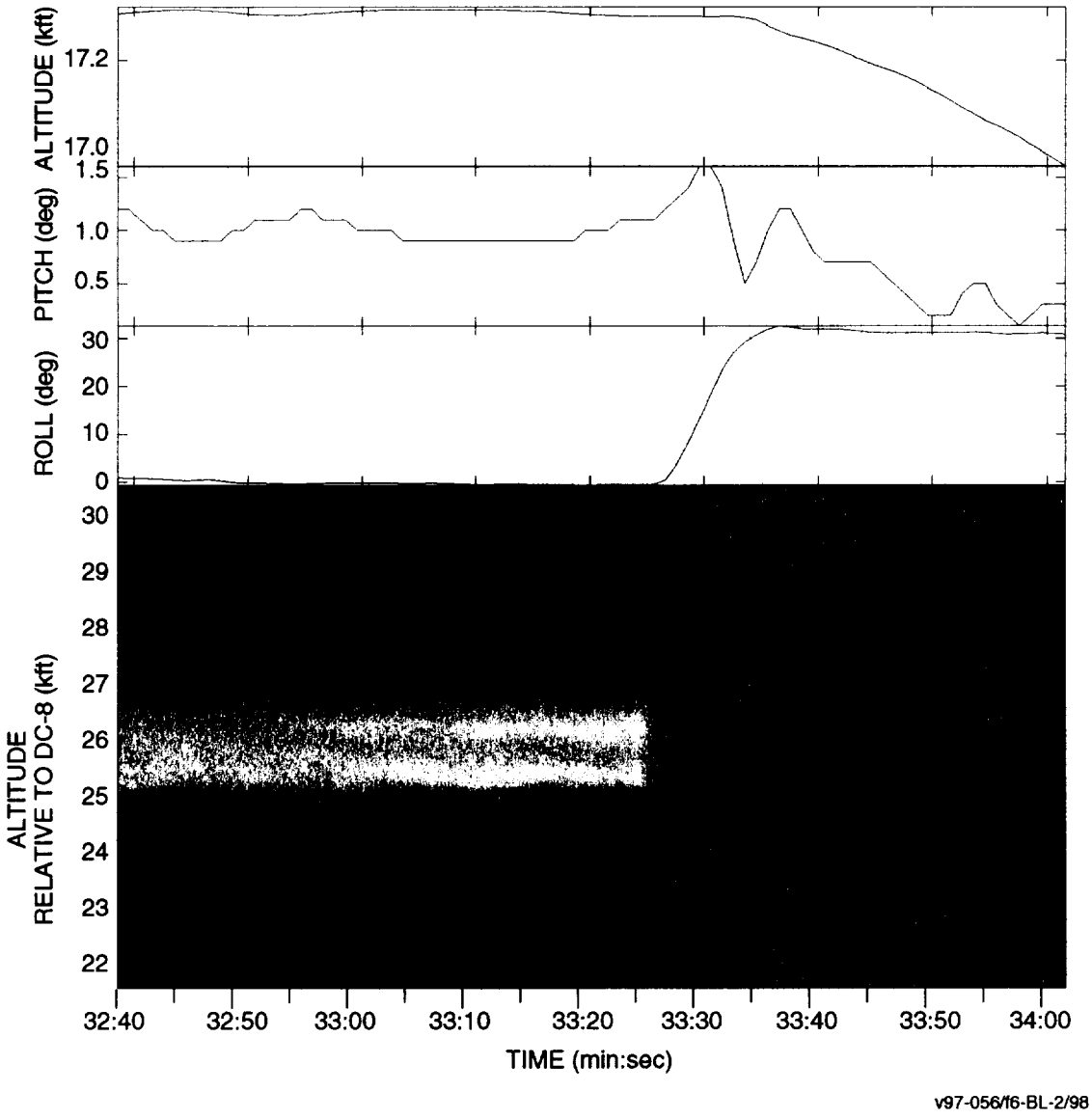

Figure 10 DC-8 LIDAR OBSERVATIONS AND SELECTED DC-8 FLIGHT PARAMETERS SHOWING A SHARP DECREASE IN LIDAR BACKSCATTER FROM A HIGH ALTITUDE (43 kft) LAYER AT SMALL ANGLES FROM THE VERTICAL, 10 MAY 1996, 16:32:40 TO 16:34:05 GMT

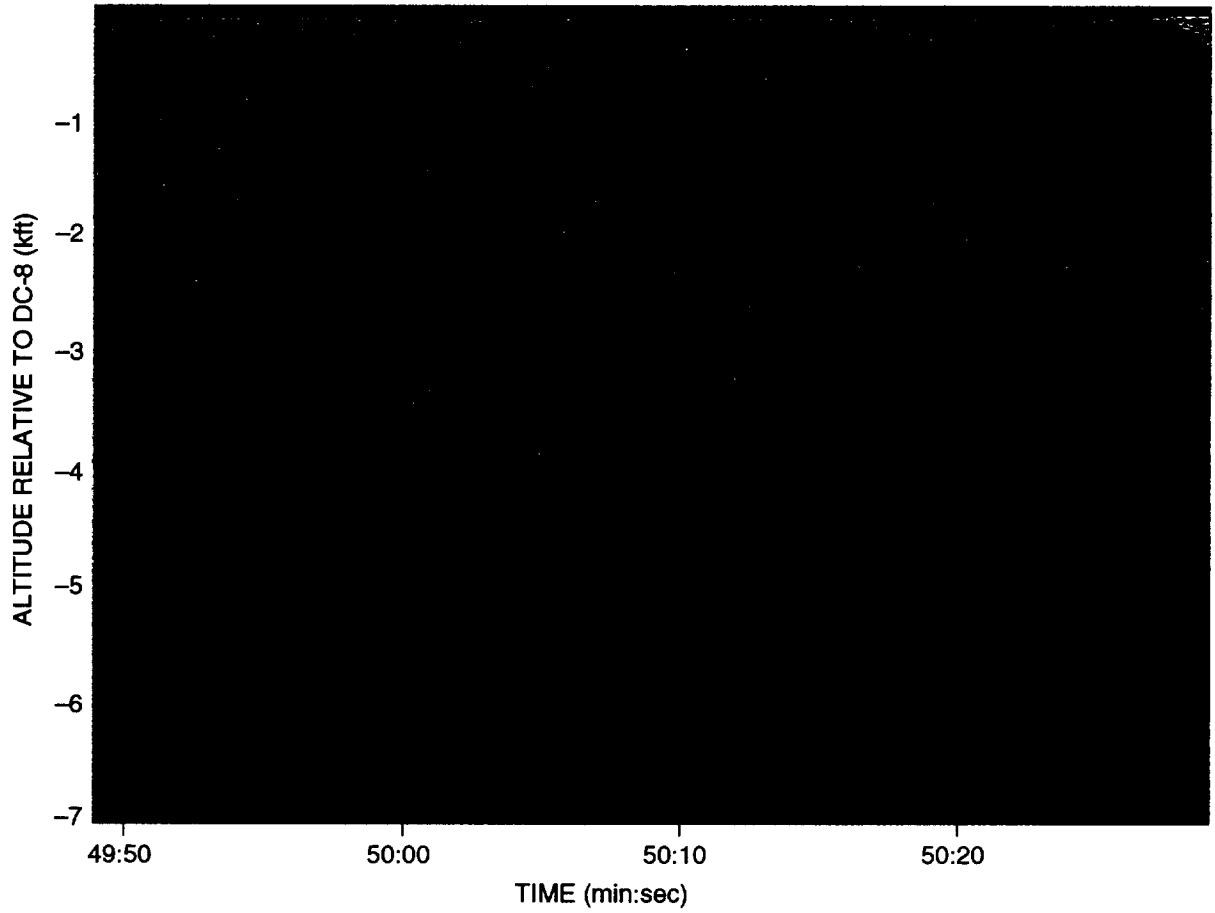

Figure 11 DC-8 DOWNWARD-VIEWING LIDAR OBSERVATIONS SHOWING INTENSE SINGLE-PIXEL RETURNS FROM PRECIPITATING ICE CRYSTALS THAT ARE SCAVAGED BY A CIRRUS CLOUD LAYER, 12 MAY 1996, 23:49:50 TO 23:50:29 GMT (DC-8 altitude approximately 39 kft)

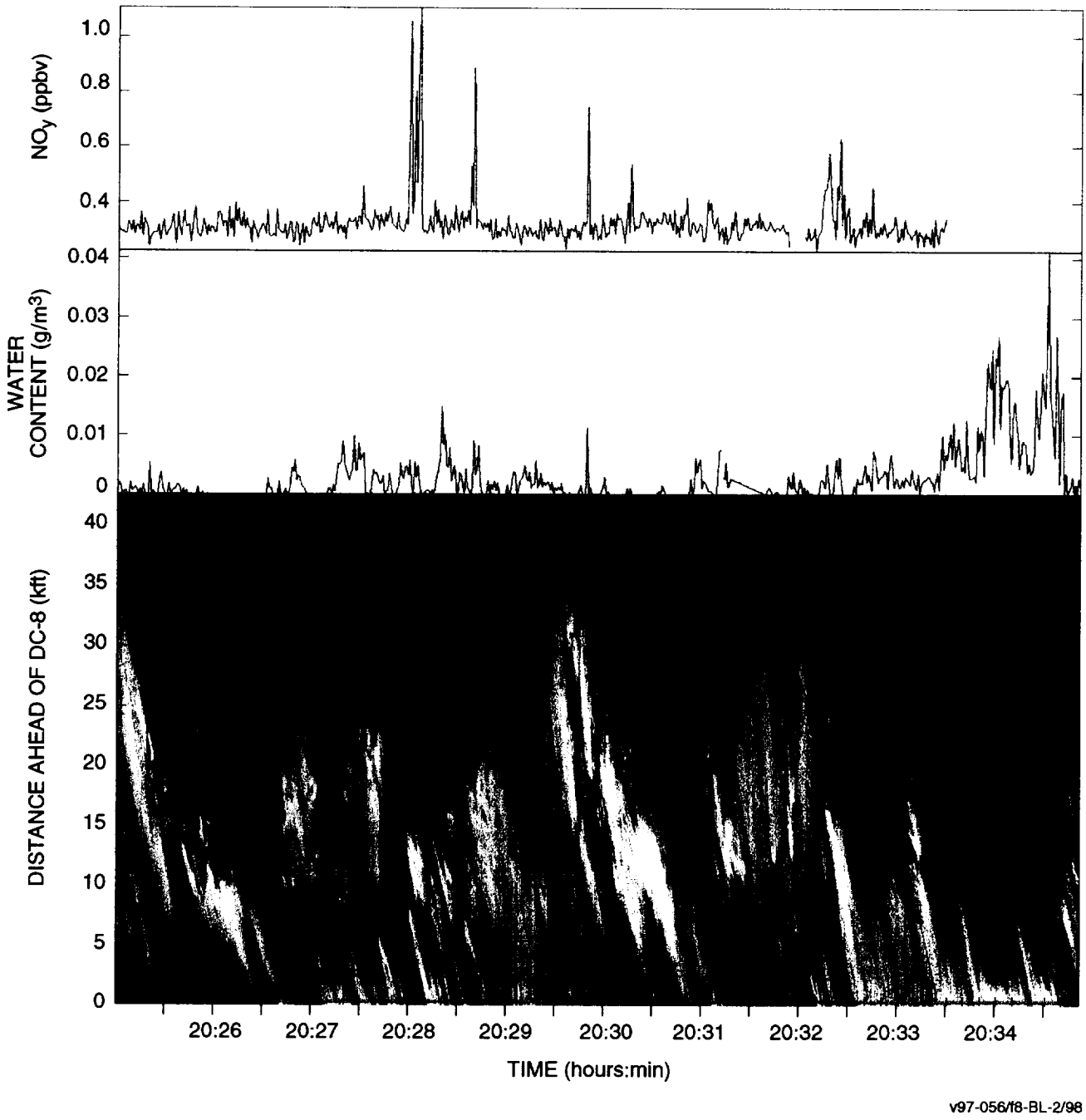

Figure 12 DC-8 FIXED-ANGLE FORWARD-VIEWING LIDAR AND SELECTED IN SITU DATA, 20 APRIL 1996, 20:25 TO 20:35 GMT (DC-8 altitude approximately 37 kft)

The above data example was used to develop a journal presentation.[2] Additional data examples are presented at web site address http://www.rsed.sri.com/lidar. Table 5 lists selected time periods for case study analyses. A proposal has been submitted to NASA to extend the data analyses products in support of AEAP model development and validation, and these results will be available at the above noted web site.

[2] Uthe, E. E., N. B. Nielsen and T. E. Osberg, 1998: "Airborne scanning lidar observations of aircraft contrails and cirrus clouds during SUCCESS," accepted for publication, *GRL*.

Table 5

SELECTED CASE STUDIES

DATE	TIME (GMT)	MODE	TAPE	REMARKS
4/10	2421–2454	–3°, +5°	1	Long range DC-8 contrail
4/13	1803–1813	+90°	1	40 kft cirrus
	1901–1902	–4°, +10°	2	Cloud scan
	1917–1931	–4°, +10°	3	41 kft cirrus
4/16	1958–2004	–3°, +10°	2	Contrail over CART
	2056–2104	–3°, + 2°	3	CART site
4/18	1939–1941	–4°, +5°	1	Cirrus penetration
	1955–2005	–4°, +5°	2	Cirrus penetration
4/20	1806–1824	–4°, +10°	3	Cirrus/contrail
	1859–1093	0°, +10°	5	Cirrus
	2025–2047	0°	5	
4/21	1807–1809	–1°, + 9°	1	Cirrus
	1856–1900	–4°, +10°	3	Cirrus
	2109–2125	–4°, +8°	10	Contrail
	?	–4°, +8°	6	DADS not recorded
	?	–4°, +8°	8	DADS not recorded
4/24	1714–1716	–4°, +7°	1	Cloud structure
	1721–1723	–4°, +7°	1	Cloud structure
	1940–1947	–1°, +5°	4	Contrails
	2040–2052	+90°	5	Cirrus
	2107–2117	0, +8°	6	–
	2122–2124	0, +8°	6	–
	2248–2255	–3°, +5°	8	Good contrails at 41 kft
	2301–2324	0°	8	Clouds
4/27	1655–1706	–4°, +5°	1	Good contrails (T-39)
	1840–1844	–2°, +10°	1	Large ice crystals
	1946–2016	–4°, +5°	1	Radiation box
	2035–2045	–4°, +5°	1	Good clouds
	2106–2109	–4°, +5°	1	Contrail
4/27	2156–2158	–4°, +10°	1	One 25° scan
	2123–2125	–4°, +10°	1	–
4/30	1809–1815	+90°	2	Radiation run
	1907–1910	+90°	3	Contrail
	1912–1916	+90°	3	Cloud/contrail
	1942–1945	+90°	3	DC-8 contrail
	2139–2150	+90°	3	Cloud above troposphere
	2200–2205	+90°	3	Cloud 3 kft above a/c
	2222–2224	+90°	3	41 kft cloud

Table 5

SELECTED CASE STUDIES
(concluded)

DATE	TIME (GMT)	MODE	TAPE	REMARKS
5/2	1637–1647	+90°	1	Contrails
	1702–1712	+90°	1	–
	1712–1722	+90°	1	–
	1723–1733	+90°	1	–
	1733–1740	+90°	1	–
	1805–1817	–90°	1	–
5/3	1934–1946	–4°, +4°	1	757 Contrails
	2023–2034	–4°, +4°	1	–
	2202–2212	–90°	1	Multiple cloud layers
	2219–2229	–90°	1	–
5/4	1744–1750	+90°	1	757 Contrails
	1900–1908	–4°, 0°	1	–
	1917–1924	–4°, 0°	1	Close in 757 contrails
	2006–2014	–4°, 0°	1	Best data for day?
5/8	1719–1729	+90°	1	Cirrus/APD gain changes
	1737–1749	+90°	1	Calibration data
	1832–1840	+90°	1	Calibration data
	1930–1941	+90°	1	35 kft alt/anvil cloud
	2028–2042	+90°	1	A/C in top of cloud
	2046–2053	–90°	1	41 kft a/c altitude
5/10	1514–1526	+90°	1	44 kft layer/39 kft altitude
	1533–1543	+90°	1	44 kft layer/31 kft altitude
	1549–1559	+90°	1	44 kft layer/28 kft altitude
	1607–1615	+90°	1	44 kft layer/23 kft altitude
	1622–1634	+90°	1	A/C turn/17 kft altitude
	1639–1644	+90°	1	44 kft layer/13 kft altitude
5/12	2045–2055	+90°	1	Cirrus
	2253–2303	+90°	1	–
	2313–2400	–90°	1	DC-8 contrails
	0010–0020	–90°	1	Cloud structure
	0035–0045	–90°	1	Within cloud
5/15	2012–2014	+90°	1	Cloud over water
	2022–2032	–90°	1	–
	2043–2053	–90°	1	–
	2055–2104	–90°	1	–
	2245–2255	+90°	1	–
	2340–2350	–90°	1	Multiple clouds over water

5 CONCLUSIONS

SUCCESS afforded the opportunity to develop and apply a scanning lidar from the NASA DC-8 atmospheric research aircraft. The lidar was able to map particulate backscatter above, ahead of, and below the DC-8 in real time for operational purposes to best position the aircraft for in situ atmospheric sampling. The recorded lidar records are also useful for interpretation of data collected from in situ and radiometric sensors and for inferring optical and radiative properties of clouds and contrails. Several interesting data products relating to the AEAP have been presented in this report and these and additional products, as they are developed, will be available at web site: http://www.rsed.sri.com/lidar.

6 ACKNOWLEDGMENTS

The SUCCESS DC-8 scanning lidar program was funded under Cooperative Agreement NCC2-885 with the NASA Ames Research Center. The water content data were provided by H. Gerber [personal communication, 1997; Gerber et al., 1998], the NO_y data by A. Weinheimer [personal communication, 1997; Ridley et al., 1994], and the solar flux records by F. Valero and A. Bucholtz [personal communication, 1997; Valero et al., 1997]. A Heymsfield suggested and encouraged analysis of the 12 May data, which proved beneficial to the program. The authors thank the many NASA DC-8 research facility staff and contractors who helped design, develop, and install the scanning lidar system, and the SUCCESS management team for their patience and support during system development.

7 PUBLICATIONS AND PRESENTATIONS

7.1 JOURNAL PUBLICATIONS

Aviontion Week and Space Technology, 1996: "NASA completes tests on airborne lidar," AW&ST, 29 July 1996 (See Appendix C).

Uthe, E. E., N. B. Nielsen, and T. E. Osberg, 1998: "Airborne scanning lidar observations of aircraft contrails and cirrus clouds during SUCCESS," accepted for publication, GRL.

7.2 CONFERENCE PRESENTATIONS

Nielsen, N. B., E. E. Uthe, R. D. Kaiser, M. A. Tucker, J. E. Baloun and J. G. Gorords, 1996: "NASA DC-8 airborne scanning lidar sensor development," Proceedings Second International Airborne Remote Sensing Conference and Exhibition, San Francisco, Calfironia, 24-27 June 1996. Available from ERIM International, Ann Arbor, MI 48113-4008.

Nielsen, N. B. and E. E. Uthe, 1996: "NASA DC-8 airborne scanning lidar system," 18th International Laser Radar Conference, 22-26 July 1996, Berlin, Germany.

Uthe, E. E., T. E. Oseberg,. and N. B. Nielsen, 1997: "NASA DC-8 airborne scanning lidar cloud and contrail observations," Proceedings, Cloud Impacts on DoD Operations and Systems 1997 Conference (CIDOS-97), 23-25 September 1997, Newport, RI. Phillips Laboratory, Directorate of Geophysics, Hanscom AFB, MA 01731-3010.

Uthe, E. E., 1997: "NASA DC-8 airborne scanning lidar operation during SASS/ SUCCESS," Abstract Volume, 1997 Conference on the Atmospheric Effects of Aviation, 10-14 March 1977, Virginia Beach, VA.

REFERENCES

Gerber, H. et al., Measurement of wave cloud microphysics with two new aircraft probes, *Geophys. Res. Lett.*, accepted for publications, GRL, 1998.

Intrieri, J.M. et al., Multiwavelength observations of a developing cloud system: The FIRE II 26 November 1991 core study, *J. Atmos. Sci.*, 4079–4093, 1995.

Measures, R.M., *Laser Remote Sensing Fundamentals and Applications,* John Wiley and Sons, New York, 1984.

Platt, C.M.R., Lidar backscatter from horizontal ice crystal plates, *J. Appl. Meteor.*, 482–488, 1978.

Ridley, B.A. et al., Distributions of NO, NO_x, NO_y, and O_3 to 12 km altitude during the summer monsoon season over New Mexico, *J. Geophys. Res.*, 99, 25519–25534, 1994.

Thomas, L. et al., Lidar observations of the horizontal orientation of ice crystals in cirrus clouds, *Tellus*, 211–216, 1990.

Uthe, E.E. and P.B. Russell, Lidar observations of tropical high-altitude cirrus clouds, *Radiation in the Atmosphere,* H.J. Bolle (Editor), Science Press, Princeton, New Jersey, 242–244, 1977.

Valero, F.P.J. et al., The Atmospheric Radiation Measurements Enhanced Shortwave Experiment (ARESE): experimental and data details, submitted to *J. Geophys. Res.*, 1997.

Appendix A

DC-8 INTEGRATION QUESTIONNAIRE

NASA Ames Research Center
Medium Altitude Missions Branch

DC-8 Integration Questionnaire

Contact Information:

Investigator: Dr. Edward Uthe Title/Affiliation: Principal Scientist

Mailing Address: SRI International
333 Ravenswood Avenue
Menlo Park, CA 94025

Telephone: (415) 859-4667 Fax: (415) 324-1369

E-Mail Box Names: Uthe@sri.com

Alternate Contact: Norm Nielsen
(415) 859-2841

Payload Information:

Experiment Name: LIDAR

Preferred sensor location on aircraft:
Right side reinforced window optical port
Station 1290 (alternate station 890)

Sensor (or optical table, etc.) size and weight:
27 x 43 x 18 in approximately 200 lbs
on top of a medium or low rack

Number, preferred location, and weight of support equipment racks:
Sensor rack at station 1290 (approximately 100 lbs equipment in rack)
Approximately 160 lb power supply in the cargo bay
Mirror and scanner outsdie of aircraft approximately 100 lbs

Where and when are racks needed for equipment installation?

SRI International
Attn: Norm Nielsen, MS-306
333 Ravenswood Avenue
Menlo Park, CA 94025

Number and location of operator seat units:
2 each station 1330

Viewport, Sensor, Probe, and Antenna Requirements:

Port size and location; equipment to be installed at port:

(First missions) location 1290/right side/15 in clear aperature
Station #8 upward
Station #9 downward

Future missions may require different optical glass windows

Optical window size; optical passband; preferred material and coating:

15 x 15 in clear aperature
1064 nm wavelength
high energy AR coating

Air sampling probes; size and orientation:

Antenna(s) size, location and orientation; RF power and frequency:

Window cleaning, probe covering, or other operational requirements:

The scanner window should be cleaned and perhaps covered when not in use

Heliostats or other special equipment; supplier:

High energy AR coatings can be supplied by CVI Laser Corporation

Electrical Power Requirements:

115 V 60 Hz, Single Phase:

Load Name	Start Current	Run Current	Comments
Lidar System	(approx. 3 Kw)	36A	No initial surge

115V 400 Hz, Three Phase:

Load Name	Start Current	Run Current	Comments

Other Electrical Power Requirements:

Load Name	Frequency	Voltage	Current	Comments

DADS (Data Acquisition and Distribution System) Requirements:

Special parameters desired: Data system supplied with lidar

Inflight data distribution rate; outlet box location(s):

Postflight data products desired:

Video or Photo Requirements:

Camera type(s), location, FOV, duration, exposure rate (if film):

Video monitor location(s) on rack(s):

1. We will need to mount 2 (lidar) video terminals on the station bulkhead.
2. We will supply a video signal available to the cockpit

Laser Systems:

Laser type, class, wavelength, and output power or energy/pulsewidth/rep rate:

ND:YAG / IV/ 1064 nm / 275 mJ / 10 ns / 10 Hz

Is laser considered eye safe per ANSI Z136.1-1986?

No

Class II (or higher) lasers, not permanently contained within an instrument, will require a laser safety plan and approval from the ARC Non-ionizing Radiation Safety Committee. Please outline safety features here:

All laser radiation within the aircraft will be contained. The transmitted beam will be directed at AZ angle away from the A/C and other protruding sensors. Electrical and/or mechanical stops will limit the scanning angles.

Compressed Gas Requirements:

List each; identify if toxic, flammable, or O2 depleting:

None

Quantity required, per flight (and per week for ground support):

Proposed storage method(s):

Corrosive, Toxic, or Flammable Materials Requirements:

List material(s) and use:

None

Quantity required per flight (and per week for ground support):

Proposed storage method(s):

Experiment Special Requirements:

(Heating or cooling; permissible temperatures, humidity, vibration, attitude; warmup or cooldown times; pre or post flight calibration, lab space during deployment, etc.)

CRYOGENICS: TYPE, AMOUNT PER WEEK.

Flight Requirements:

(Range, altitude, speed, altitude profiles, precision patterns or ground tracks, etc.)

Cargo Shipment Requirements:

Experiment Participants:

Name	Affiliation and Citizenship	at ARC	Transit Flights	Data Flights
2 of the following 3				
Norm Nielsen	SRI, USA			
Robert Kaiser	SRI, USA			
Edward Uthe	SRI, USA			

(Please also fill out and return the attached Visit Information Sheet, Form ARC-127, listing all experimenters who will require admission to Ames Research Center at any time during the experiment program.)

Miscellaneous Requirements and Other Comments:

The side window installation will require a motor driven scanning mirror in the forward direction from -4 degrees to +10 degrees and tilted away from the A/C at approximately 2 degrees. The scanning mechanism will be located exterior to the A/C optical window port at station 1290 on the right side.

Checklist for Experimenter Furnished Documentation:

Integration Questionnaire
ARC-127, Visit Information Sheet
Engineering Drawings
Stress Reports
Rack Loading
Laser and/or Radiation Safety Plan
Toxic/Flammable Safety Plan

NASA Ames Telephone Exchange:

ARC Telephone System numbers: (415)604-xxxx

NASA Ames DC-8 Contacts:

John Reller	DC-8 Project Manager	-5392
~~Leo DeGreef~~	~~DC-8 Mission Manager~~	~~-5342~~
Chris Scofield	DC-8 Mission Manager	-4599
Bob Morris	DC-8 Mission Manager	-5476
Bob Davidson	NSI Integration Engineer	*(415)962-7030
Mike Tucker	NSI Integration Engineer	*(415)962-7028
Jack Baker	NSI Mission Planner	-4260
OMM FAX		-3885
OMM Office		-5336

LASER USER EXPERIENCE RECORD

NAME Norman Nielsen ORG CODE 714

1. TRAINING

TYPE OF TRAINING COURSE	WHERE TRAINED	DURATION OF TRAINING	ON THE JOB FORMAL (circle one)	
Engineering, Physics, Biology, etc.	SRI International	many weeks	YES NO	YES NO
Laser Courses	ILS Laser Systems Orlando, Florida	1 week	YES NO	YES NO
Laser Safety Courses	ILS Laser Systems Orland, Florida	1 day	YES NO	YES NO

2. LASER EXPERIENCE

TYPE OF LASER	POWER	USE (CHEMICAL ANALYSIS DISTANCE MEASURING, ETC.)	DURATION OF EXPERIENCE
Nd:YAG Excimer Ruby CO_2 HF/DF (and others	200 MW	Atmospheric Research	30 years

3. RECEIPT OF REGULATIONS

I have read and understood the following material:

( ) Ames Health and Safety Manual, Chapter 8 / Lasers & Microwaves

DATE _____ SIGNATURE _____

DQS-29 (3/88)

RADIATION SAFETY COMMITTEE LASER INVENTORY

HP#_____

ORG._____ AUTHORIZED LASER USER_____

BLDG._____ ROOM NO._____ DATE _____ CLASS _____

1. Description of Laser
   - A. TYPE Nd:YAG
   - B. MANUFACTURER Spectra-Physics
   - C. MODEL/SERIAL DCR-11/3-333
   - D. ARC # _____
   - E. WAVE LENGTH EMITTED 1064nm
   - F. MAXIMUM OUTPUT 275 mJ
   - G. BEAM DIAMETER 6 mm
   - H. BEAM DIVERGENCE <0.5 mrad

2. Other Users of Laser _____

3. Description of Use
   Atmospheric Lidar Sensor

4. Safety Features
   - A. SHIELDING Yes
   - B. WARNING DEVICES Yes
   - C. INTERLOCKS Yes
   - D. SPECIAL OPERATING PROCEDURES
     A test plan will be submitted
   - E. CLASSIFICATION LABEL Class IV

5. Eye Protection
   - A. TYPE OF EYEWEAR eye wear will be provided for maintenance
   - B. WAVELENGTH MARKED ON EYEWEAR _____
   - C. OPTICAL DENSITY (OD) _____
   - D. SPECIAL PROVISIONS _____

6. Special Hazards _____

_____ _____

DATE SIGNATURE OF PERSON RESPONSIBLE FOR LASER

_____ _____

DATE RADIATION SAFETY OFFICER

DQH-27(3/88)

Appendix B

AIRBORNE LIDAR EXPERIMENT PLAN

AIRBORNE LIDAR EXPERIMENT PLAN

Principal Investigators:

Edward E. Uthe (415 859 4667) and Norman B. Nielsen (415 859 2841)

Affiliation:

SRI International, Geoscience and Engineering Center, 333 Ravenswood Ave, Menlo Park California, 94025

General Description:

The SRI/DC-8 Scanning Lidar system has been developed for characterization of aircraft contrails and cirrus clouds. In order to assess the atmospheric impact of subsonic aircraft, a scanning mirror pod is attached to the DC-8 aircraft. This provides for scanning lidar observations over a small angular sector (15°) vertically overhead and forward of the DC-8, and fixed angle upward or downward observations as shown in the following illustration (Figure 1).

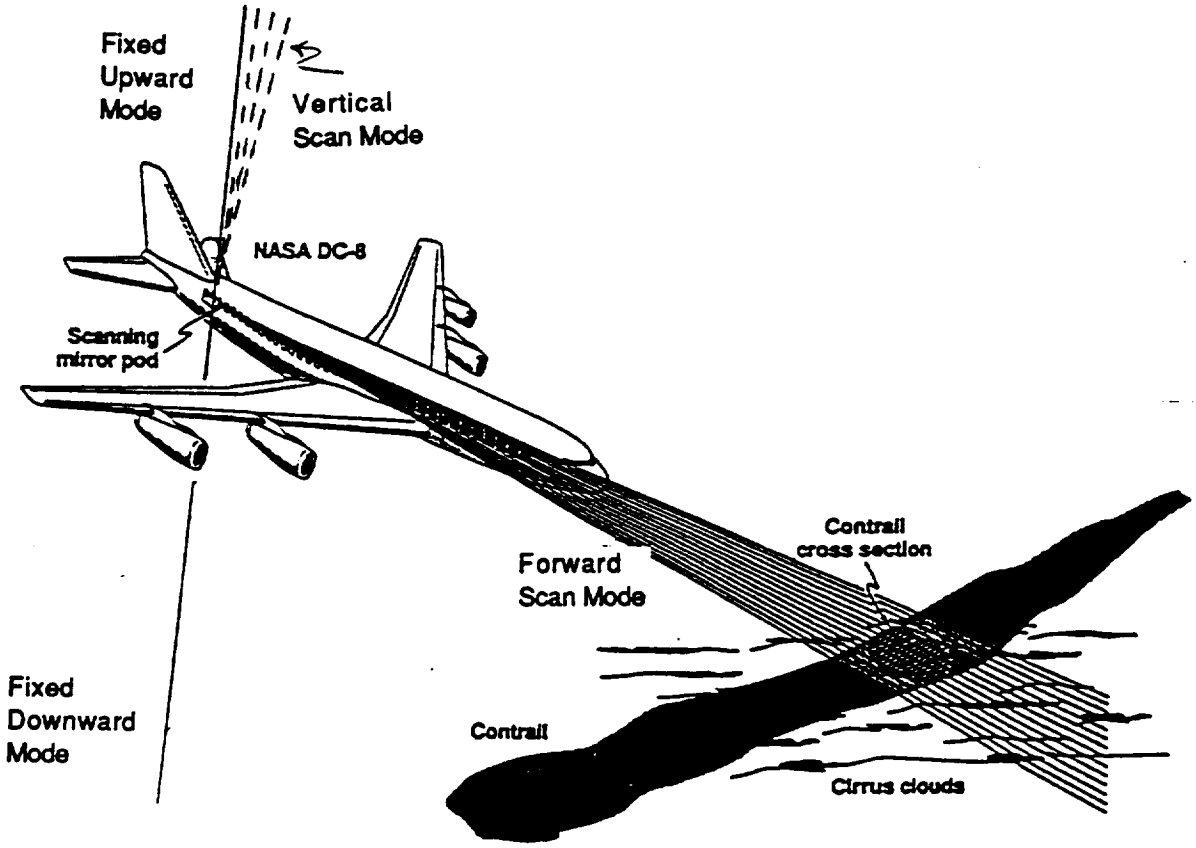

The lidar assembly is constructed on a single DC-8 low instrumentation rack at station 1290. A previous lidar system (NASA Langley Aerosol Lidar) with very similar specifications was flown at this same location in 1993. This lidar system employs a commercial

(un-modified) ND:YAG laser (model DCR-11) that has been previously flown on an Air Force C-130 aircraft for similar atmospheric testing. The lidar transmitter is a completely self contained Class IV laser and its specifications are listed in Table 1. The laser beam is not exposed inside the DC-8 aircraft.

Purpose:

The purpose of this lidar system is to aid in the study of chemistry within clouds and aircraft contrails with the following objectives:

- Map contrail/cloud vertical distributions ahead of DC-8
- Provide DC-8 guidance into enhanced scattering layers
- Document DC-8 flight path intersection of contrail and cloud geometry's
- Analyze contrail/cloud radiative properties
- Evaluate mean particle sizes of aircraft emissions from two-wavelength observations
- Study contrail/cloud interactions, diffusion, and mass decay/growth
- Make observations in the near-field of aircraft emissions

Schedule of operation:

February 26 - March 24	• Equipment Installation and integration.
March 24 - March 27	• Power-up and vertical optical alignment checkout from the runway apron and/or horizontal alignment to a fixed target parallel to a closed runway.
March 28 - April 8	• Aircraft test flights.
April 9 - May 9	• Data flights from Salina Kansas.
May 13 - May 17	• Remove equipment from DC-8.

Initial calibration and alignment:

All ground operations requiring turn on of the laser transmitter while the DC-8 is on the ground, will proceed only with approval of the DC-8 flight manager and appropriate flight and airport control authorities. After lidar installation aboard the DC-8, and prior to any mode of lidar operation, SRI will conduct a hardware alignment and calibration procedure consisting of the following:

- An observer will be posted outside the aircraft with established radio or intercom to the lidar operator and wearing eye safety glasses. He will have a disable control switch that will prevent firing of the lidar at his discretion.
- The scanning mirror pod will be manually pointed downward (nadir) at a diffuse surface material laying on the ground.

- The laser will be operated in a long pulse mode, (200 μsec rather than the normal 10 nsec Q switched mode) which along with reduced lamp energy is relatively eye safe.
- The laser lamp energy will be reduced to operational threshold, so that the green light is just barely visible to the lidar operator.
- A single laser pulse will be fired using a manual push button control, so that the laser operator can look for the back reflection from the anti-reflection coated optical scanner window and install a beam stop in front of the telescope. This beam stop is for a technical purpose and the entire area will be completely enclosed during normal operation.
- The laser pulse rate frequency (PRF) will then be increased to 1 Hz and the color video camera cross hairs will be aligned with the green long pulse on the diffuse surface at the ground. (approximately 30 min. test)
- The lidar will be turned off and the scanner will then be positioned to direct the lidar beam onto a solid target located on the side of an un-manned truck approximately 150 ft forward, and viewed above the wing of the aircraft. The lidar beam will be completely blocked by the target and will not hit the wing of the aircraft. The lidar will be turned on and the camera cross hairs will be re-adjusted.
- With the lidar off, the target vehicle will be moved to a longer distance, (approximately 500 m - 1km) and the alignment will be verified. The laser will be operated in a Q-switched mode and the energy increased to a level that provides good lidar returns for receiver calibration.
- All interested parties will be informed when the calibration is complete. (approximately 1-2 hr test)

Ground operational procedures: (NASA Ames and Salina Airports)

Mode 1. Vertical cirrus cloud observation.

During alignment and evaluation of the lidar in a fixed vertical upward position, (zenith) an observer will be posted outside the DC-8 to look for aircraft that might be approaching the area. The observer will be in radio contact with the airport control tower during the test. When an all-clear is given to the lidar operator from the observer, the lidar will be powered on for the test. The observer will continue to look for aircraft and the lidar will be immediately turned off at the request of the tower or observer. The control tower will be notified upon completion of the testing. Mode 1.

operational time requirements may extend from a few minutes for calibration / maintenance operations to several hours for cirrus cloud data collection.

Mode 2. Horizontal target calibration.

The DC-8 will be parked on a closed taxi way and the lidar will be pointed in a fixed horizontal position looking forward of the aircraft. A solid calibration target fixed to a truck will be positioned at approximately 1 km from the lidar and will completely stop the lidar beam. An observer with radio contact with the tower will be posted as in mode 1, to observe any approaching vehicles. Operational periods of the lidar will be controlled at the request of the tower and observer.

Airborne operational procedures:

All lidar operations during DC-8 flights will be approved and coordinated by the Mission Manager. Status of the lidar will be available at all times through the on-board communications. The lidar operations can be terminated at any time with a control switch located at the Mission Manager station or the lidar operator.

Mode 1. Forward scanning.

This mode of operation will only be conducted when the DC-8 is flying in class A air space and adequate eye hazard distance between aircraft can be maintained.

The lidar will be computer controlled to scan forward of the DC-8, within the angular sector of -4° to +10°. The scanning pod is designed to direct the lidar beam away from the fuselage of the DC-8 at a 2° angle to avoid interference with other sensors. Attachment Figure 2 illustrates the lidar viewing paths for viewing angles of -4 to +10°. The figure establishes the eye hazordous region above and below the aircraft during Mode 1 operation and will be used to limit the angular scan sector in restrictive flight areas. Tabulations of values are given in attachment Table 2.

Mode 2. Upward vertical fixed zenith position.

During this mode of operation the scanner pod is locked in a fixed upward position. The DC-8 traveling in a forward direction allows the lidar to collect cloud data in the atmosphere above the aircraft.

Mode 3. Upward vertical Scanning.
This mode of operation will only be used for a special test in which the lidar will scan vertically within the angular sector of zenith and 15° forward.

Mode 4. Downward fixed nadir position.
The testing in this configuration will use only the 1064 nm wavelength when the aircraft is greater than 31,000 ft above ground level so that the lidar beam is eye save at the ground level.(see NOHD attachment) This test will be coordinated to collect atmospheric data below the DC-8 for comparison with ground based lidar systems.

NOTE- Operational safeguards have been established and will be implemented for all modes of operation. (see safeguards)

Potential hazards:

The following table lists the lidar Transmitter Specifications.

Table 1 - Airborne Lidar Transmitter Parameters

	Nd:YAG	Doubled Green
Wavelength	1064 nm	532 nm
Energy per pulse	275 mJ	(1 wavelength)
Energy per pulse	130 mJ	130 mJ (2 wavelength)
Rep rate	10 pps	10 pps
Pulse width	10 nsec	10 nsec
Beam divergence	0.5 mr	0.5 mr
Beam diameter	6.4 mm	6.4 mm

Based on the above specifications the maximum permissible exposure (MPE) for this system is:

Wavelength	MPE*
532 nm	3.98×10^{-7} J/cm^2
1064 nm	1.58×10^{-6} J/cm^2

*See attachment for calculations

The Nominal Optical Hazard Distance (NOHD) for this system is:

Wavelength	NOHD*	
	2 wavelength (upward & forward scan)	1 wavelength (down / up and forward)
532 nm	12.9 km (42,323 ft.)	
1064 nm	6.46 km (21,194 ft.)	9.39 km (30,807 ft.)

*See attachment for calculations

Safeguards:

The following safeguards and operating procedures will be in place during all lidar operations:

- All high voltage enclosures are safety interlocked and will only be accessible for maintenance by authorized personnel.
- The lidar beam is completely enclosed and can only exit the aircraft through the scanner pod window.
- A lidar inhibit switch installed at the Mission Manager station allows the lidar operation to be immediately terminated at any time by either the manager or the lidar operator. The Mission Manager and the lidar operator will be in communication through the on-board intercom at all times.
- A color video camera is installed in the scanner pod and will track the target area as the lidar scans. A cross hair cursor is superimposed on the video scene and bore sighted with the center of the lidar beam. The camera field of view (20° H x 15° V) is much larger than the lidar beam divergence (0.5 mill radians). In the event of an approaching aircraft the lidar beam will be extinguished by the operator before the aircraft gets near the target area. The video will be monitored by the lidar operator prior to, and during all lidar operation to insure that the test area is clear.

- A second video camera located in the DC-8 cockpit will provide a view ahead of the aircraft on a video display at the mission manager (Safety Officer) station. The mission manager will grant permission over the intercom for lidar operation to begin, only when it is safe to do so, and terminate lidar operation at any time.

- Scanning of the lidar is computer controlled and the direction of the lidar beam is verified by an optical encoder. In the event of an electrical malfunction a mechanical stop will limit the scanning.

- For upward or downward fixed operation the scanning pod is mechanically locked into position.

- For all ground based testing a person will be designated as an observer to watch the lidar path and give an all-clear to the lidar operator.

Quality Assurance:

At the time of hardware installation on the DC-8 aircraft, and before any ground based or airborne testing is conducted, an inspection of the lidar equipment and it's installation will be conducted by representatives of the Ames Research Center Laser Safety Committee. The lidar system will also be inspected by representatives of the Ames Air worthiness Review Panel.

Key Personnel:

At all times during the use of this lidar equipment the operations will be supervised by either Dr. Edward Uthe, Principal Investigator, or Norm Nielsen, Senior Research Engineer from SRI International. These people are Authorized Laser Users (ALU) as defined by ARC regulations. In addition, the DC-8 Mission Manager, who has overall authority for the facility operation will serve as Safety Officer.

NASA Review:

This experiment is in review by the Ames Research Center Laser Safety Committee (LSU). All aspects of the design, installation and operation procedures are reviewed. No operations will be conducted prior to final approval.

This experiment is also in review by the ARC Aircraft Flight Safety Review Panel (AFSRP). No aircraft operations (ground or flight missions) are conducted prior to final approval.

Attachments:

MPE Analysis Calculations:

NOHD Analysis Calculations:

Figure 2 Angular Hazard in Flight Plot

Table 2 Angular Hazard in Flight Tabulation

Additional Safety Comments:

MPE Analysis

ALU SRI ALPHA-IA Laser Type Nd:YAG

Wavelength 532 nm
Pulse Energy 0.130 Joules
Pulse Length 10×10^{-9} seconds
Beam Divergence 0.5×10^{-3} Radians
Beam Diameter 0.64 cm
n (n=PRF x T_{max}) 2.5 pulses

MPE 5×10^{-7} Joules/cm^2
Time (t) 10×10^{-9} seconds
T_{max} 0.25 seconds
PRF 10 Hz
$n^{-1/4}$ 0.795
$Power_{avg}$ 1.3 Watts

MPE: H = 5×10^{-7} J/cm^2

$\therefore$ MPE/Pulse: $H \leq n^{-1/4} \times H$

$\leq 0.795 \times 5 \times 10^{-7}$ J/cm^2

$= 3.975 \times 10^{-7}$ J/cm^2

MPE/(cum): $H \leq (T_{max}) \times (PRF) \times (H)$

$= 9.94 \times 10^{-7}$ J/cm^2

MPE: $E = H/T = 3.975 \times 10^{-6}$ W/cm^2

MPE 3.975×10^{-6} W/cm^2

Nominal Ocular Hazard Distance (NOHD)

MPE $_{pulse\ train}$ 3.975×10^{-6} W/cm^2

Power$_{avg}$ 1.3 Watts

Pulse Energy 0.130 Joules

Diameter 0.64 cm

Beam Divergence 0.5×10^{-3} Radians

MPE $_{per\ pulse}$ 3.975×10^{-7} J/cm^2

$$r_{NOHD\ SinglePulse} = \frac{1}{\phi}\left(\sqrt{\frac{4}{\pi} x \frac{Q}{MPE}} - Diameter\right)$$

$$= \frac{1}{0.5 \times 10^{-3}}\left(\sqrt{\frac{4}{\pi} x \frac{0.130\ J}{3.975 \times 10^{-7}\ J/cm^2}} - 0.64\ cm\right)$$

$= 1.29 \times 10^{6}$ cm $= 1.29 \times 10^{4}$ m

$$r_{NOHD\ T_{max}} = \frac{1}{\phi}\left(\sqrt{\frac{4}{\pi} x \frac{\Phi}{MPE}} - Diameter\right)$$

$$= \frac{1}{0.5 \times 10^{-3}}\left(\sqrt{\frac{4}{\pi} x \frac{1.3\ W}{3.975 \times 10^{-6}\ W/cm^2}} - 0.64\ cm\right)$$

$= 1.29 \times 10^{6}$ cm $= 1.29 \times 10^{4}$ m

NOHD $_{per\ pulse}$ 1.29×10^{4} m

NOHD $_{Tmax}$ 1.29×10^{4} m

MPE Analysis

ALU SRI ALPHA-IA Laser Type Nd:YAG

Wavelength 1064 nm
Pulse Energy 0.130 Joules
Pulse Length 10×10^{-9} seconds
Beam Divergence 0.5×10^{-3} Radians
Beam Diameter 0.64 cm
n (n=PRF x T_{max}) 100 pulses

MPE 5×10^{-6} Joules/cm^2
Time (t) 10×10^{-9} seconds
T_{max} 10 seconds
PRF 10 Hz
$n^{-1/4}$ 0.316
$Power_{avg}$ 1.3 Watts

MPE: H = 5×10^{-6} J/cm^2

$\therefore$ MPE/Pulse: $H \leq n^{-1/4} \times H$

$\leq 0.316 \times 5 \times 10^{-6}$ J/cm^2

$= 1.58 \times 10^{-6}$ J/cm^2

MPE/(cum): $H \leq (T_{max}) \times (PRF) \times (H)$

$= 1.58 \times 10^{-4}$ J/cm^2

MPE: $E = H/T = 1.58 \times 10^{-5}$ W/cm^2

MPE 1.58×10^{-5} W/cm^2

Nominal Ocular Hazard Distance (NOHD)

MPE $_{pulse\ train}$ 1.58×10^{-5} W/cm^2

Power$_{avg}$ 1.3 Watts

Pulse Energy 0.130 Joules

Diameter 0.64 cm

Beam Divergence 0.5×10^{-3} Radians

MPE $_{per\ pulse}$ 1.58×10^{-6} J/cm^2

$$r_{NOHD\ SinglePulse} = \frac{1}{\phi}\left(\sqrt{\frac{4}{\pi} x \frac{Q}{MPE}} - Diameter\right)$$

$$= \frac{1}{0.5 \times 10^{-3}}\left(\sqrt{\frac{4}{\pi} x \frac{0.130\ J}{1.58 \times 10^{-6}\ J/cm^2}} - 0.64\ cm\right)$$

$= 6.46 \times 10^{5}$ cm $= 6.46 \times 10^{3}$ m

$$r_{NOHD\ T_{max}} = \frac{1}{\phi}\left(\sqrt{\frac{4}{\pi} x \frac{\Phi}{MPE}} - Diameter\right)$$

$$= \frac{1}{0.5 \times 10^{-3}}\left(\sqrt{\frac{4}{\pi} x \frac{1.3\ W}{1.58 \times 10^{-5}\ W/cm^2}} - 0.64\ cm\right)$$

$= 6.46 \times 10^{5}$ cm $= 6.46 \times 10^{3}$ m

NOHD $_{per\ pulse}$ 6.46×10^{3} m

NOHD $_{Tmax}$ 6.46×10^{3} m

MPE Analysis

ALU SRI ALPHA-IA

Laser Type Nd:YAG

Single Wavelength Operation

Wavelength 1064 nm

Pulse Energy 0.275 Joules

Pulse Length 10×10^{-9} seconds

Beam Divergence 0.5×10^{-3} Radians

Beam Diameter 0.64 cm

n (n=PRF x T_{max}) 100 pulses

MPE 5×10^{-6} Joules/cm^2

Time (t) 10×10^{-9} seconds

T_{max} 10 seconds

PRF 10 Hz

$n^{-1/4}$ 0.316

$Power_{avg}$ 2.75 Watts

MPE: H = 5×10^{-6} J/cm^2

$\therefore$ MPE/Pulse: $H \leq n^{-1/4} \times H$

$\leq 0.316 \times 5 \times 10^{-6}$ J/cm^2

$= 1.58 \times 10^{-6}$ J/cm^2

MPE/(cum): $H \leq (T_{max}) \times (PRF) \times (H)$

$= 1.58 \times 10^{-4}$ J/cm^2

MPE: $E = H/T = 1.58 \times 10^{-5}$ W/cm^2

MPE 1.58×10^{-5} W/cm^2

Nominal Ocular Hazard Distance (NOHD)

Single wavelength (1064 nm) Operation

MPE $_{pulse\ train}$ 1.58×10^{-5} W/cm^2

Power$_{avg}$ 2.75 Watts

Pulse Energy 0.275 Joules

Diameter 0.64 cm

Beam Divergence 0.5×10^{-3} Radians

MPE $_{per\ pulse}$ 1.58×10^{-6} J/cm^2

$$r_{NOHD\ SinglePulse} = \frac{1}{\phi}\left(\sqrt{\frac{4}{\pi} x \frac{Q}{MPE}} - Diameter\right)$$

$$= \frac{1}{0.5 \times 10^{-3}}\left(\sqrt{\frac{4}{\pi} x \frac{0.275\ J}{1.58 \times 10^{-6}\ J/cm^2}} - 0.64\ cm\right)$$

$= 9.40 \times 10^{5}$ cm $= 9.40 \times 10^{3}$ m

$$r_{NOHD\ T_{max}} = \frac{1}{\phi}\left(\sqrt{\frac{4}{\pi} x \frac{\Phi}{MPE}} - Diameter\right)$$

$$= \frac{1}{0.5 \times 10^{-3}}\left(\sqrt{\frac{4}{\pi} x \frac{2.75\ W}{1.58 \times 10^{-5}\ W/cm^2}} - 0.64\ cm\right)$$

$= 9.40 \times 10^{5}$ cm $= 9.40 \times 10^{3}$ m

NOHD $_{per\ pulse}$ 9.40×10^{3} m

NOHD $_{Tmax}$ 9.40×10^{3} m

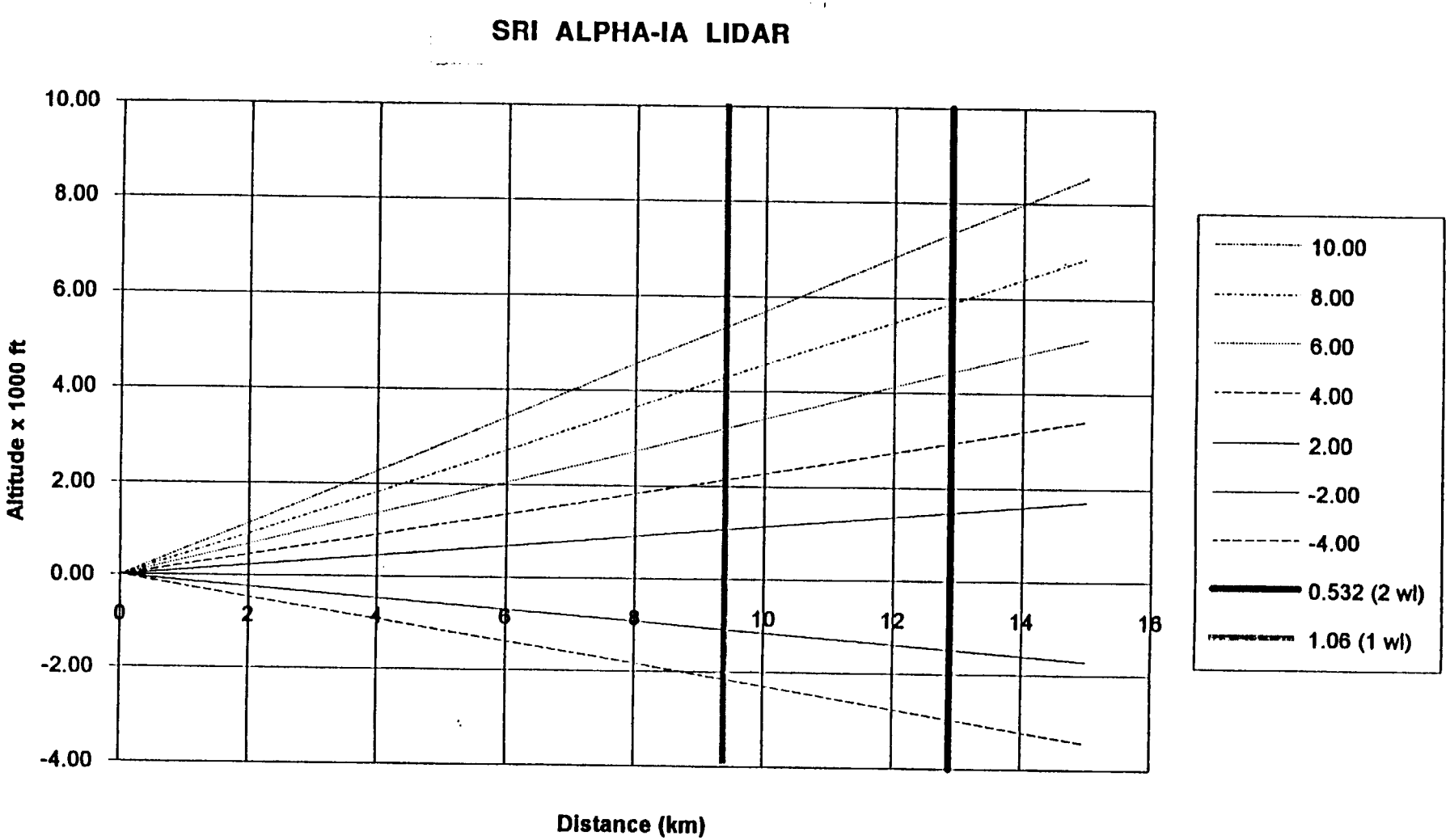
SRI ALPHA-IA LIDAR
10.00
8.00
6.00
4.00
2.00
0.00
-2.00
-4.00
Altitude x 1000 ft
0
2
4
6
8
10
12
14
16
Distance (km)
10.00
8.00
6.00
4.00
2.00
-2.00
-4.00
0.532 (2 wl)
1.06 (1 wl)

Figure 2

Table 2

ALPHA-IA LIDAR Eye Safety Analysis

Altitude (ft) vs. Scan Elevation(deg) for various Distances (km)

	Distance (km)		
Scan Angle (deg)	6.50	9.40	12.90
-4	-1491.56	-2157.03	-2960.18
-2	-746.24	-1079.18	-1481.00
0	0.00	0.00	0.00
2	746.24	1079.18	1481.00
4	1491.56	2157.03	2960.18
6	2235.06	3232.24	4435.74
8	2975.82	4303.50	5905.86
10	3712.94	5369.48	7368.75

Altitude (kft) vs. Distance (km) for various Elevation values

	Scan Elevation (degrees)							
Distance (km)	10.00	8.00	6.00	4.00	2.00	0.00	-2.00	-4.00
0	0.00	0.00	0.00	0.00	0.00	0.00	0.00	0.00
1	0.57	0.46	0.34	0.23	0.11	0.00	-0.11	-0.23
2	1.14	0.91	0.69	0.46	0.23	0.00	-0.23	-0.46
3	1.71	1.37	1.03	0.69	0.34	0.00	-0.34	-0.69
4	2.28	1.83	1.37	0.92	0.46	0.00	-0.46	-0.92
5	2.85	2.28	1.71	1.14	0.57	0.00	-0.57	-1.14
6	3.42	2.74	2.06	1.37	0.69	0.00	-0.69	-1.37
7	3.99	3.20	2.40	1.60	0.80	0.00	-0.80	-1.60
8	4.56	3.65	2.74	1.83	0.92	0.00	-0.92	-1.83
9	5.13	4.11	3.09	2.06	1.03	0.00	-1.03	-2.06
10	5.70	4.57	3.43	2.29	1.14	0.00	-1.14	-2.29
11	6.27	5.02	3.77	2.52	1.26	0.00	-1.26	-2.52
12	6.84	5.48	4.11	2.75	1.37	0.00	-1.37	-2.75
13	7.40	5.93	4.46	2.97	1.49	0.00	-1.49	-2.97
14	7.97	6.39	4.80	3.20	1.60	0.00	-1.60	-3.20
15	8.54	6.85	5.14	3.43	1.72	0.00	-1.72	-3.43

Additional Safety Comments:

There are several operational parameters that favor overall eye safe conditions for **lidar** operation that are not taken into consideration when calculating the laser hazard. Some of these are:

- The calculations are based on the maximum available energy that the laser can provide as specified by the laser manufacture. In reality, the laser is built into a lidar system and there are energy losses on all of the beam steering optics and windows prior to the beam being emitted into the atmosphere. As the laser operates the flash lamps and optics slowly deteriorate and the output energy can be considerably less than in it's original condition.
- Atmospheric attenuation and scattering along the beam path to the target is very significant and is not considered at all in the hazard calculations.
- The fact that the lidar beam is scanning and the DC-8 platform is moving at a considerably speed, makes it highly unlikely that more than one pulse of light can strike an eye, but the hazard calculations assume multiple exposure.
- In the case of hitting another aircraft, the windows of most airplanes have some curvature or surface angle that would deflect part of the collimated light. Also the window surfaces are not anti-reflection coated at a given laser wavelength or made of optical quality materials so that attenuation of the beam is significant.
- Due to the scientific nature of this particular lidar program it is not expected that the lidar system will be used during nighttime conditions, and "cockpit illumination" at the visible 532 nm wavelength will not be a factor. If nighttime observations are required during the missions, only the 1064 nm wavelength laser energy will be transmitted.
- The "flash blindness" range for the visible 532nm (based on 5μ Watts/cm^2) is 11.5 km. We have chosen to use the longer more conservative eye hazard range (NOHD) of 12.9 km in the safety operations plan.

Appendix C

"NASA COMPLETES TESTS ON AIRBORNE LIDAR"

(Aviation Week and Space Technology, 29 July 1996)

NASA Completes Tests On Airborne Lidar

PAUL PROCTOR/SEATTLE

Details of a lidar (laser radar) scanning mirror pod installed near the tail of NASA's DC-8 atmospheric research aircraft shows the rotating mirror in a stowed position (photo, right) as well as pod internal and aerodynamic fairing structure (photo below). Yarn filaments are for testing the pod's effect on airflow.

The lidar-equipped DC-8, operated by NASA's Ames Research Center, completed a five-week flight program in April and May along with other aircraft as part of NASA's Subsonic Aircraft Contrail and Cloud Effects Special Study (Success). The project investigated cirrus clouds and aircraft contrails using a variety of sensors. It is part of NASA's larger Atmospheric Effects of Aviation Program.

High altitude visible and subvisible cirrus clouds and contrails consisting of ice crystals of various sizes and shapes can effect propagation of visible and infrared energy. This may influence global climate as well as performance of ballistic missile flights, infrared targeting sensors and atmospheric laser beam defense systems.

THE DC-8'S SCANNING lidar system was supplied and operated by SRI International, Menlo Park, Calif. It comprises four modules: two-channel Spectra Physics neodymium-doped yttrium aluminum garnet laser transmitter, telescope receiver, scanning mirror pod and data acquisition, processing and display system. The lidar functions by measuring backscatter from suspended particulate matter.

The lidar's avionics modules are mounted in a standard DC-8 equipment rack. A separate laser power supply and heat exchanger package is mounted directly on seat rails.

Although similar to equipment used in previous fixed-angle airborne lidar studies, the co-axial receiver field of view and laser beam are directed through an aircraft side open window port to the scanning pod. The pod consists of a rotating cylindrical housing with an embedded 45-deg. mirror and a 17-in. optical side window treated with antireflection coating, according to Norman B. Nielsen, senior research engineer at SRI's Geoscience and Engineering Center.

THE POD IS PRESSURIZED to avoid laser beam routing through an optical window at the fuselage surface.

The computer-controlled, motor-driven lidar scanner can view from straight up to forward to straight down with a gap caused by the aircraft's wing. The lidar provides a real-time display of atmospheric structure, according to Edward E. Uthe, principal scientist at SRI's Geoscience and Engineering Center.

Lidar's ability to determine the presence, altitude and thickness of particulate layers above and below the DC-8 helps researchers establish optimal altitudes for in-situ aerosol and gas chemistry sampling. The lidar performs forward-looking angular scan patterns to map the vertical structure of clouds and contrails the DC-8 is about to penetrate.

NASA NOW IS ANALYZING a large volume of cirrus cloud and contrail observation data acquired by the lidar and other sensors during the Success tests. The data pictured shows, from top to bottom, intensity modulated radar display with a scale ranging from 10,000 ft. above the aircraft and up to 15-km. (9.3-mi) ahead; infrared and visible (green wavelength) lidar backscatter logarithmic intensity plotted as a function of range; text box detailing time and aircraft position data. The clouds shown in this example extend to an altitude of 41,700 ft. above sea level.

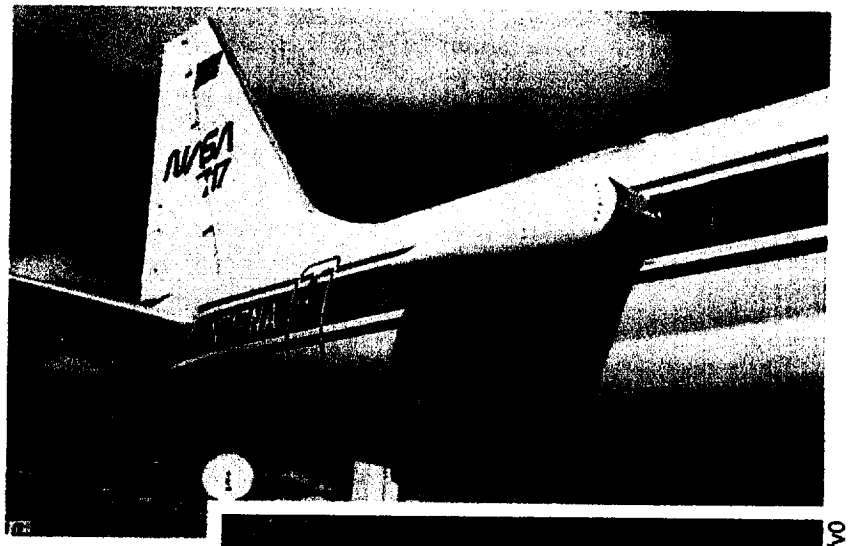

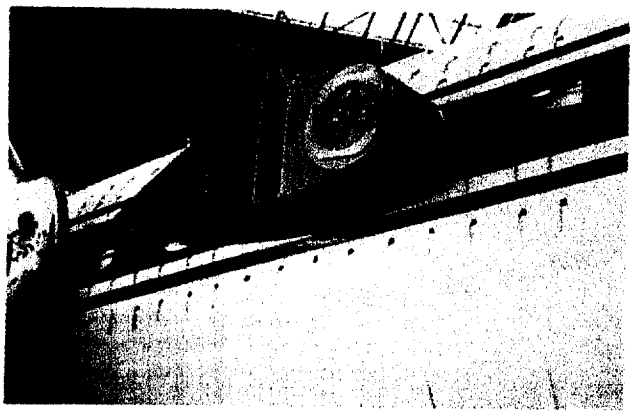

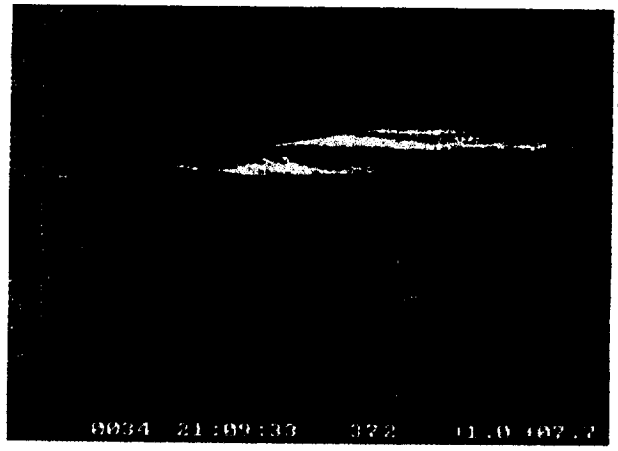

OV-052-96A